Upregulated Ca^{2+} release from the endoplasmic reticulum leads to impaired presynaptic function in Alzheimer's disease

Temitope Adeoye[1], Syed I Shah[1], Angelo Demuro[2], David A Rabson[1], and Ghanim Ullah[1,*]

[1]Department of Physics, University of South Florida, Tampa, FL 33620.

[2]Department of Neurobiology and Behaviour University of California, Irvine, CA 92697.

[*]Correspondence: gullah@usf.edu

Abstract

Neurotransmitter release from presynaptic terminals is primarily regulated by rapid Ca^{2+} influx through membrane-resident voltage-gated Ca^{2+} channels (VGCCs). Also, accumulating evidence indicates that the endoplasmic reticulum (ER) is extensively present in axonal terminals of neurons and plays a modulatory role in synaptic transmission by regulating Ca^{2+} levels. Alzheimer's disease (AD) is marked by enhanced Ca^{2+} release from the ER and downregulation of Ca^{2+} buffering proteins. However, the precise consequence of impaired Ca^{2+} signalling within the vicinity of VGCCs (active zone (AZ)) on exocytosis is poorly understood. Here, we perform in-silico experiments of intracellular Ca^{2+} signalling and exocytosis in a detailed biophysical model of hippocampal synapses to investigate the effect of aberrant Ca^{2+} signalling on neurotransmitter release in AD. Our model predicts that enhanced Ca^{2+} release from the ER increases the probability of neurotransmitter release in AD. Moreover, over very short timescales (30-60 msec), the model exhibits activity-dependent and enhanced short-term plasticity in AD, indicating neuronal hyperactivity—a hallmark of the disease. Similar to previous observations in AD animal models, our model reveals that during prolonged stimulation (~450 msec), pathological Ca^{2+} signalling increases depression and desynchronization with stimulus, causing affected synapses to operate unreliably. Overall, our work provides direct evidence in support of a crucial role played by altered Ca^{2+} homeostasis mediated by intracellular stores in AD.

Introduction

Alzheimer's disease (AD) is the most common and burdensome of the late-onset degenerative dementias: the world Alzheimer report estimated a global prevalence of over 50 million worldwide, a number expected to triple by 2050 [85, 86]. AD manifests as progressive memory impairment initially and faster rate of cognitive decline and neurodegeneration in later stages. Despite the convoluted etiology of AD, experimental and theoretical investigation suggests that synapses are the primary targets in the early stage of the disease [87, 88]. Histologically, the AD brain is marked by extracellular deposition of senile beta-amyloid (Aβ) plaques—the result of abnormalities in the genes encoding amyloid precursor protein (APP) or intramembrane protease presenilin 1 and 2 (PS1, PS2). These are accompanied by intracellular accumulation of neurofibrillary tangles (NFTs)—composed of hyperphosphorylated tau proteins (pTau)—that litter the cerebral and hippocampal cortices [89—93]. Although the exact mechanism is still being debated, numerous experimental studies implicate elevated intracellular Ca^{2+} levels as one of the main mechanisms underlying Aβ toxicity [94, 95]. These studies show that the AD brain is surfeit with dysregulation of Ca^{2+} signalling pathways [94—97], motivating researchers to propose the Ca^{2+} hypothesis of AD and aging [126]. Indeed, it has been shown that both intra- and extracellular Aβ oligomers and familial AD (FAD)-causing mutations in presenilin cause enhanced Ca^{2+} release from the ER through inositol (1, 4, 5)-triphosphate (IP_3) receptors (IP_3Rs) and/or ryanodine receptors (RyRs) [16, 17, 94—100, 127—129]. This upregulated Ca^{2+} release can contribute to aberrant plasticity and functional disruption of neuronal networks [44, 95].

Intracellular Ca^{2+} is an important second messenger for regulating a multitude of neuronal functions, including neurotransmitter release. Synaptic function at nerve terminals is tightly coupled to intracellular Ca^{2+} concentration ($[Ca^{2+}]$), as Ca^{2+} primarily regulates the biological machinery responsible for exocytosis and short-term plasticity [28, 29]. The precise temporal control of synaptic transmission by Ca^{2+} is achieved via local signal transduction mechanisms that aim to regulate Ca^{2+} excitability at the axonal bouton. Voltage-gated Ca^{2+} channels (VGCCs) are the primary mediators of the transduction of depolarization-induced Ca^{2+} transients into neurotransmitter release. Furthermore, Ca^{2+} influx through VGCCs leads to physiological events that alter plasma membrane functions underpinning synaptic plasticity, protein expression, spine maintenance, and regulation of excitability in excitatory synapses [45, 46]. Likewise, investigations of the Ca^{2+}-dependence of vesicular release have highlighted

the role of intracellular stores in Ca^{2+} handling and spontaneous exocytosis [21, 47]. Thus, the close association between these Ca^{2+} pathways, their effect on numerous neuronal processes, and their high sensitivity to pathological perturbations makes it especially valuable to elucidate the exact nature of the coupling.

Extensive evidence supports the presence of the ER in the nerve terminal of CA3 pyramidal neurons [21, 47, 44, 101—103]. In neurons, activation of Ca^{2+}-sensitive channels like IP_3Rs and RyRs triggers the release of Ca^{2+} from the ER. Opening of IP_3Rs primarily depends on Ca^{2+} and IP_3. To achieve this, glutamate released into the synaptic cleft elicits the production of IP_3 by the activation of membrane-bound mGLuRs. RyRs activation, on the other hand, is largely controlled by cytosolic [Ca^{2+}]. This specialized cascade underscores the importance of IP_3Rs and RyRs in the regulation of the Ca^{2+} induced Ca^{2+} release (CICR) mechanism of the ER. Previous works have shown that CICR is necessary for ER stores to adequately influence spontaneous vesicle release and homosynaptic plasticity [21, 104]. Indeed, *in vitro* studies confirm that properly sensitized CICR is necessary for normal synaptic function, whereas aberrant CICR underlies presynaptic impairment associated with AD [19, 20, 80, 82]. Despite this evidence, the precise role of ER Ca^{2+} handling in action potential (AP)-evoked presynaptic Ca^{2+} dynamics and its downstream effect on presynaptic neuronal processes remain unclear [19—21, 82].

Information encoding at the CA3 to CA1 synapses in the hippocampus, which is crucial for learning and memory storage, relies on the spatiotemporal organization of Ca^{2+} events leading up to synaptic transmission [108]. AP arrival at the nerve terminal activates VGCCs, leading to high-amplitude, short-lived Ca^{2+} influx events into the AZ. Coupled with this specialized pathway, Ca^{2+} sensors initiate a heterogeneous fusion of neurotransmitter vesicles with the plasma membrane that often culminates in either fast synchronous or slow asynchronous release. Neuronal communication primarily relies on the synchronous mode of exocytosis, which is regulated by synaptotagmin-1 (*Syt1*) sensors with low Ca^{2+} affinity and rapid kinetics that are critical for the exquisite temporal precision of vesicle fusion that characterizes synaptic transmission at most CA3-CA1 terminals [37, 62, 105]. Such a high degree of synchrony is in part achieved by the steep dose dependence of evoked release on the short-lived Ca^{2+} transients constrained to micro- or nanodomains within the vicinity of VGCCs [28, 106]. A global buildup of [Ca^{2+}], on the other hand, accelerates the recruitment of release-ready vesicles, controlling the degree of synaptic plasticity [130]. Thus, changes in Ca^{2+} signals at the local or

global scale are expected to disrupt synaptic transmission and plasticity. Consistent with this assertion, experimental manipulations that perturb evoked Ca^{2+} influx alter the contribution of the synchronous mode of release to overall exocytosis and compromise synaptic plasticity [38, 39, 107]. These findings highlight the need for a thorough investigation of the potential link between impaired synaptic function and disrupted Ca^{2+} homeostasis in AD.

In this study, we incorporate findings from extensive experimental and computational studies to develop a detailed biophysical model of Ca^{2+}-driven exocytosis at the CA3 presynaptic terminal. The model accounts for the observed Ca^{2+} and IP_3 signalling pathways necessary for intracellular Ca^{2+} regulation and integrates the elaborate kinetics of neurotransmitter release—vesicle docking, mobilization, priming, and fusion—aided by distinct Ca^{2+} sensors. We reproduced crucial statistics of both Ca^{2+} and release events reported at small excitatory synapses, such as transient timescale, amplitude, and decay time. By developing a mathematical framework for coupling the Ca^{2+} domains surrounding the ER and AZ, we study how AD-associated pathological Ca^{2+} release from the ER disrupts presynaptic neurotransmitter release rates and consequently alter synaptic plasticity and facilitation at affected synapses. Overall, our work provides novel insights on the pathologic role of aberrant neuronal Ca^{2+} handling on glutamate release and the downstream effects on synaptic dysfunction and cognitive decline observed in AD.

Results

The gain-of-function enhancement of IP_3R gating in AD

The exaggerated Ca^{2+} release observed in familial AD (FAD)-affected neurons is ascribed mainly to the gain-of-function enhancement of IP_3Rs in the affected cells due to FAD-causing mutations in presenilin [16, 17, 58, 124, 128]. Indeed, it has been shown that cell models expressing PS mutations exhibit a several-fold increase in the open probability (P_o) of IP_3Rs [17, 58]. Specifically, the P_o of IP_3R in cortical neurons from 3xTg-AD mice carrying PS mutations was enhanced by 700% relative to control mice with wildtype (WT) PS (0.43 ± 0.05 in AD versus 0.06 ± 0.01 in WT mice) at a cytosolic $[Ca^{2+}]$ ($[Ca^{2+}]_c$) of 1 μM and IP_3 concentration ($[IP_3]$) of 10 μM [58]. Given that all models for IP_3R in WT or AD-affected cells are based on non-neuronal cells, we use the above findings to build a new model for the gating

kinetics of IP_3Rs in neurons from WT and 3xTg-AD mice (see details in *Methods* section). Parameters yielding the best fit to experimental observations are listed in *Table* 6.

Our model mimics the gating of IP_3R in neurons from WT and 3xTg-AD mice (*Fig 1*), closely reproducing the observed values of the P_o (*Fig 1A, D*), mean open time (τ_o) (*Fig 1B, E*), and mean close time (τ_c) (*Fig 1C, F*) reported in [128]. The significantly higher P_o of the channel in AD-affected neurons is reflected in the time-traces from the model, showing that the channel spends significantly more time in the open state in the diseased state (*Fig 1G*). To determine how the observations about different resting $[Ca^{2+}]_C$ in AD-affected cells change the behaviour of IP_3Rs, we plot the P_o of the channel as a function of $[Ca^{2+}]_C$ and $[IP_3]$ (*Fig. 1H, I*). Previous studies of 3xTg and APP_{SW} AD mice models reported resting $[Ca^{2+}]_c$ of *247±10.1 nM* and *225.2±11.7 nM* respectively, whereas $[Ca^{2+}]_c$ of *110.8±1.5 nM* was recorded in WT mice [15]. In particular, cortical neurites of plaque bearing mice express a 6-fold increase in resting $[Ca^{2+}]_c$ relative to non-transgenic mice [55]. Here, our model exhibits a 4.42-fold increase in P_o of IP_3Rs in WT neurons as we increase $[Ca^{2+}]_c$ from *110 nM* to *250 nM* (0.005626 vs 0.02484) at 0.3 μM $[IP_3]$. At $[IP_3] = 0.3$ μM and $[Ca^{2+}]_c = 250$ nM, P_o of the channel in AD-affected neurons reaches 0.2565—a 10.32-fold increase relative to WT neurons (*Fig 1H, I*). Thus, an IP_3R in the AD-affected neurons will exhibit an almost 45-fold increase in P_o compared to control neurons with the same amount of IP_3, leading to a significantly higher Ca^{2+} release from the ER.

Characterization of the glutamate release model and release event

We next examine the relationship between total release from a single process following $[Ca^{2+}]_c$ clamps at different concentration steps. We observe that the release rate rapidly increases and transiently decays back to basal level within tens of milliseconds—a result of the sensitivity of the Ca^{2+} sensors (*Fig 2A*). For comparison, we also show the release rate given by the Allosteric model at different $[Ca^{2+}]_c$ values (*Fig. 2B*). Also, we obtain results similar to quantitative studies of transmission profiles in Calyx-of-Held synapse [1]. Unsurprisingly, we observed a shift in the $[Ca^{2+}]_c$ dependency of the peak release rate as the response to clamped intracellular Ca^{2+} levels is both lower and right-shifted relative to the experimental data for the Calyx-of-Held (*Fig 2C*), whereas the time delay (time-to-peak) of peak release rate shows higher and right-shifted exponential decay (*Fig 2D*). This is consistent with observations of approximately hundred-fold decrease in total vesicle population in hippocampal boutons [2, 3]. In addition, our model mimics the Ca^{2+}-dependent increase in peak release rate observed at high fidelity

synapses of cerebellar mossy fibre boutons (cMFBs), which permit direct presynaptic recordings and are reported to have high structural similarities with their hippocampal counterparts (*Fig 2C*) [131, 132]. Moreover, in agreement with previous recordings of spontaneous release events from CA3-CA1 synapses, we affirmed that the spontaneous release rate elicited by resting level $[Ca^{2+}]_c$ of 100 nM is within the reported range of 10^{-4} and 10^{-5} per ms [4, 5, 6]. The Dual-Sensor model is more in line with the findings on CA3-CA1 synapses, and is used for the remaining of this paper.

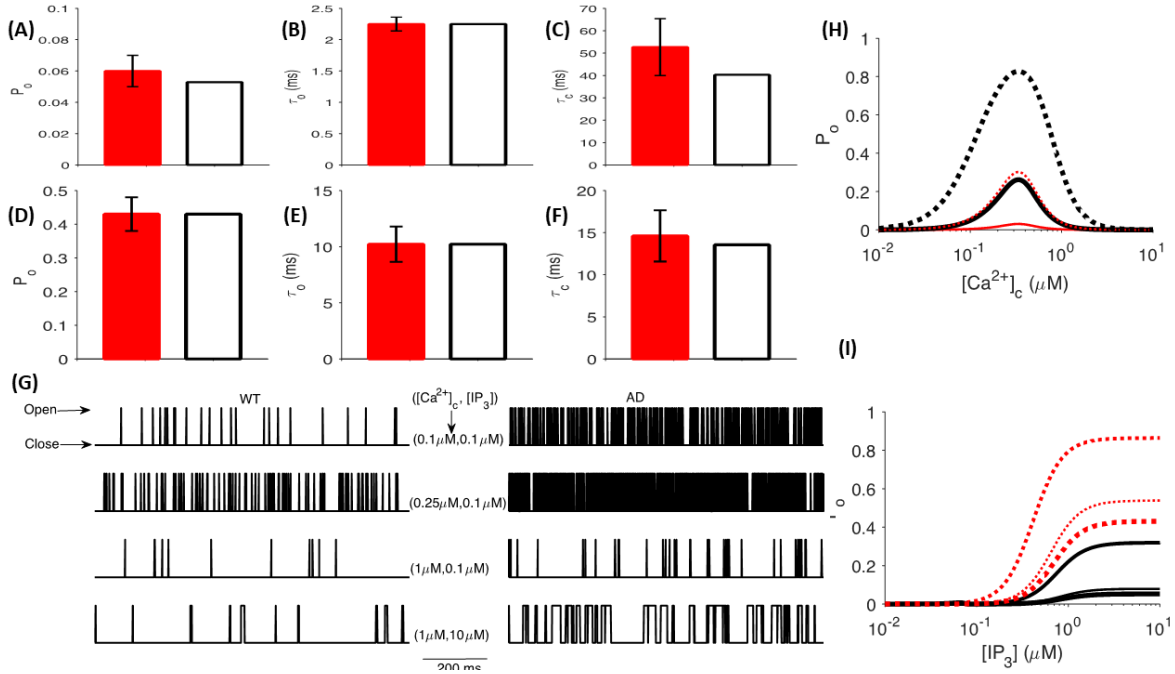

Figure 1. *Gain-of-function enhancement of IP3R gating in AD*. The P_o (A, D), τ_o (B, E), and τ_c (C, F) of IP_3R given by the model (empty bars) and observed values in primary cortical neurons from WT (A-C) and 3xTg AD mice (filled bars) (D-F) at $[Ca^{2+}]_c$ = 1 μM and $[IP_3]$ = 10 μM. (G) Sample time-traces generated by stochastically simulating a single IP_3R channel in cortical neurons from WT (left column) and AD (right column) mice at different $[Ca^{2+}]_c$ and $[IP_3]$ values shown in the figure. (H) P_o of IP_3R as a function of $[Ca^{2+}]_c$ at $[IP_3]$ = 0.3 μM (thin lines) and 1 μM (thick lines) in WT (solid lines) and AD-affected (dotted) neurons. (I) P_o of IP_3R as a function of $[IP_3]$ at $[Ca^{2+}]_c$ = 0.1, 0.25, and 1 μM (the increasing value of $[Ca^{2+}]_c$ is represented by the thickness of the line) in WT (solid lines) and AD-affected (dotted) neurons. Experimental values shown for comparison in (A-F) are from [128].

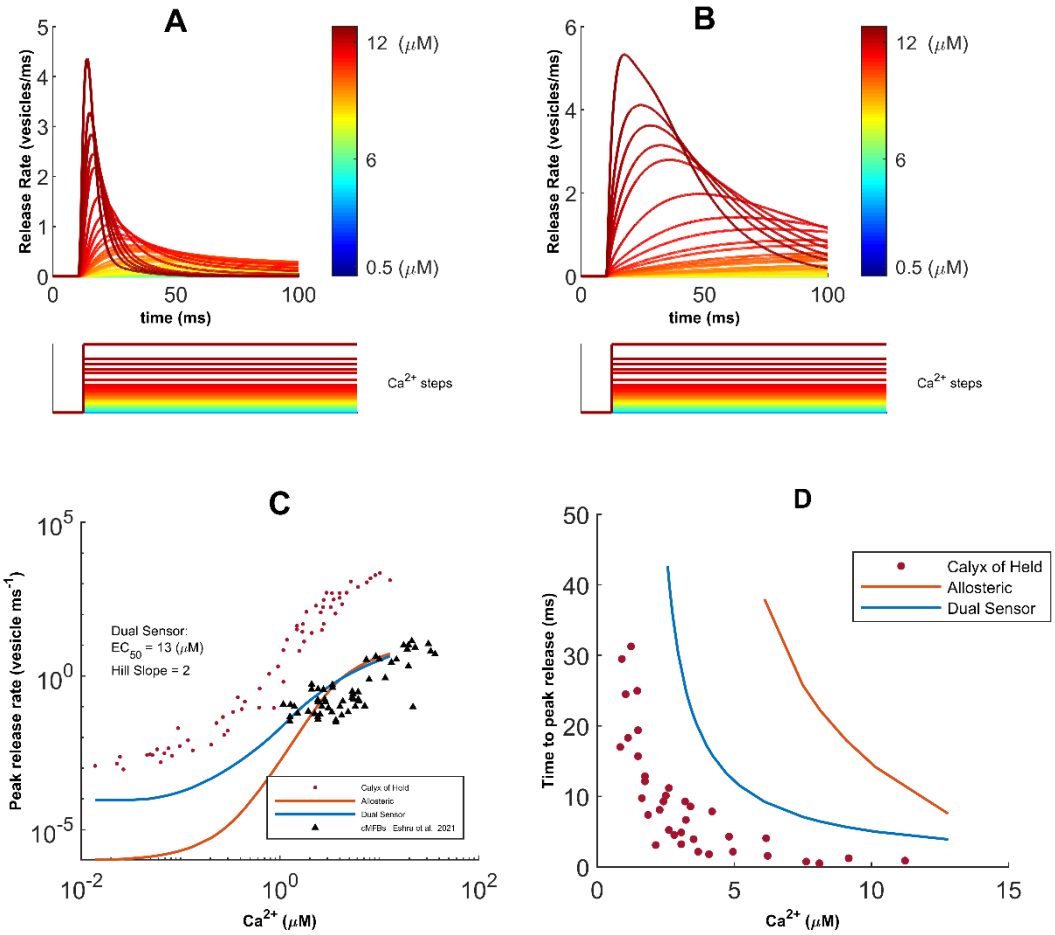

Figure 2. *Characterization of neurotransmission in response to $[Ca^{2+}]_c$ steps.* (A) Total release events obtained from a single Dual-Sensor fusion process after clamping $[Ca^{2+}]_c$ at different values. (B) Release profile following Allosteric fusion in response to stepwise $[Ca^{2+}]_c$ clamp. (C) Regulation of the peak release rate in response to clamped $[Ca^{2+}]_c$ levels show lower and right-shifted dose-responses relative to the experimental data for the Calyx-of-Held. (D) $[Ca^{2+}]_c$ dependence of time-to-peak rate indicates exponentially decreasing but longer time delay to peak release when matched with data for the Calyx-of-Held. Experimental values shown for comparison in (C, D) are from [131]

AD-associated intracellular Ca^{2+} changes enhance neurotransmitter release

Several studies have reported enhanced Ca^{2+} release from the ER in AD-affected neurons [10—14]. This enhanced Ca^{2+} release has been associated with the several fold increase in the P_O of IP_3Rs observed in multiple animal and human cell models of AD [11, 15—17, 128]. Although presynaptic plasticity and synaptic vesicle release (SVR) are tightly coupled to Ca^{2+} entry through VGCCs, several studies have established an important role for ER stores in regulating

presynaptic plasticity and neurotransmission [18—22]. Furthermore, strong experimental evidence supports the existence of a feedback loop between the ER Ca^{2+} stores and AP triggered exocytosis events [7]. Accordingly, here we explore how the observed gain-of-function enhancement of IP_3Rs in AD affects neurotransmitter release. In addition to enhanced Ca^{2+} release through IP_3Rs, multiple studies have implicated a significant downregulation of Ca^{2+} buffering proteins in AD-affected neurons as compared to WT neurons [133—135]. We incorporate the effect of observed changes in Ca^{2+} buffering proteins by considering two configurations: *High Coupling* (*HC*) and *Normal Coupling (NC)* between the ER and AZ. The *HC* configuration corresponds to the downregulation of Ca^{2+} buffering proteins (see more details in *Methods* section).

In *Fig. 3A*, we show a typical release profile in response to a single AP, where a clear difference between WT and AD-affected synapses can be seen. To quantify this difference, we compute the release probability (Pr) by counting the number of vesicles released from the slow and fast release-ready pool (RRP), divided by the number of vesicles initially in both pools. In AD-affected synapse, we observe enhanced Pr over a wide range of VGCCs' expressions in dose-response manner (*Fig 3B*), suggesting that the acute effects of AD-driven aberrant cytosolic Ca^{2+} are not exclusive to synapses operating in the regime of sparse VGCCs. Surprisingly, we observe only a marginal difference in the peak release rate between WT and AD-affected synapses *(Fig 3C)*. We also calculated the number of vesicles released during a single AP by integrating the rate of vesicle release from the slow and fast RRP, and noticed a significant increase in vesicles released in the AD-affected synapse (*Fig. 3D*). To discern the contribution of enhanced Ca^{2+} release through IP_3Rs from that due to the *HC*, we simulate four scenarios: (1) enhanced Ca^{2+} release through IP_3Rs but *NC* (AD-NC), (2) enhanced Ca^{2+} release through IP_3Rs with *HC* (AD-HC), (3) normal Ca^{2+} release through IP_3Rs and *NC* (WT-NC), and (4) normal Ca^{2+} release through IP_3Rs and *HC* (WT-HC). We notice that while *HC* causes a minor increase in the release probability and vesicles released in the WT synapse, it strongly affects both these features in the AD-affected synapse (*Supplementary Fig 1A, B*).

To gain deeper insight into the observed changes in the Pr, we examine the dependence of the release rise time (*Time to peak release rate)* on Pr (Pr is increased by increasing the number of VGCCs as in *Fig 3A*) and observed no significant differences between AD-affected and WT synapses *(Fig 3E)*. Interestingly, the decay time (*Time to basal release rate*) exhibits a biphasic dependence on Pr with a longer decay time in AD-affected synapse. Strikingly, the decay time

as well as the concomitant AD-associated enhancement is attenuated in synapses with both high and low Pr, and peaks at *Pr* corresponding to physiologically reasonable VGCCs expression for small hippocampal synapses [*35*], indicating that such small hippocampal synapses are more sensitive to alternations due to AD-associated Ca^{2+} disruptions *(Fig 3F)*. Like the release probability as a function of time and vesicles released during a single AP, HC has a stronger effect on the release rise time mainly due to the changes in Ca^{2+} in AZ in the AD-affected synapse (*Supplementary Fig 1C, D*).

To assess the direct correspondence between the changes in different aspects of SVR and enhanced Ca^{2+} release, we examine the cumulative Ca^{2+} at AZ. The elevated Ca^{2+} release from the ER maintains larger cumulative Ca^{2+} (area under the Ca^{2+} transient) at AZ in the AD-affected synapse consistently across a wide range of VGCCs expression, in agreement with several studies showing that ER Ca^{2+} channels can sculpt the spatiotemporal dynamics of exocytosis and consequently neuronal function *(Fig 3G)* [8, 9]. However, this continuous enhancement as a function of VGCCs expression is not consistent with the biphasic behaviour of the time to basal rate as a function of *Pr*. Next, we examined the residual Ca^{2+} in the AZ, obtained as the cumulative Ca^{2+} that persists during decay phase of the Ca^{2+} transient. Our results show that larger residual Ca^{2+} in AD-affected synapses also exhibits a biphasic behaviour as a function of *Pr* similar to the time to basal neurotransmitter release rate. Again, this enhancement was non-uniform, suggesting that small hippocampal synapses with intermediate *Pr* values are highly sensitive to pathological alterations *(Fig 3H)*. Taken together, our data reveal that ER-driven Ca^{2+} disruption plays a critical role in shaping the observed response profile, with the acute effects induced by such disruptions more severely expressed in small hippocampal synapses. Our results also show that these effects are more sensitive to the coupling between the Ca^{2+} domains in the vicinity of VGCCs and ER in AD-affected synapses (*Supplementary Fig 1C, D*), consistent with reports on the involvement of ER Ca^{2+} in the regulation of presynaptic resting $[Ca^{2+}]_c$ and neurotransmission [7—9]. Furthermore, the sensitivity to the coupling between the Ca^{2+} domains is exacerbated for synapses with intermediate *Pr* values (*Supplementary Fig 1C, D*).

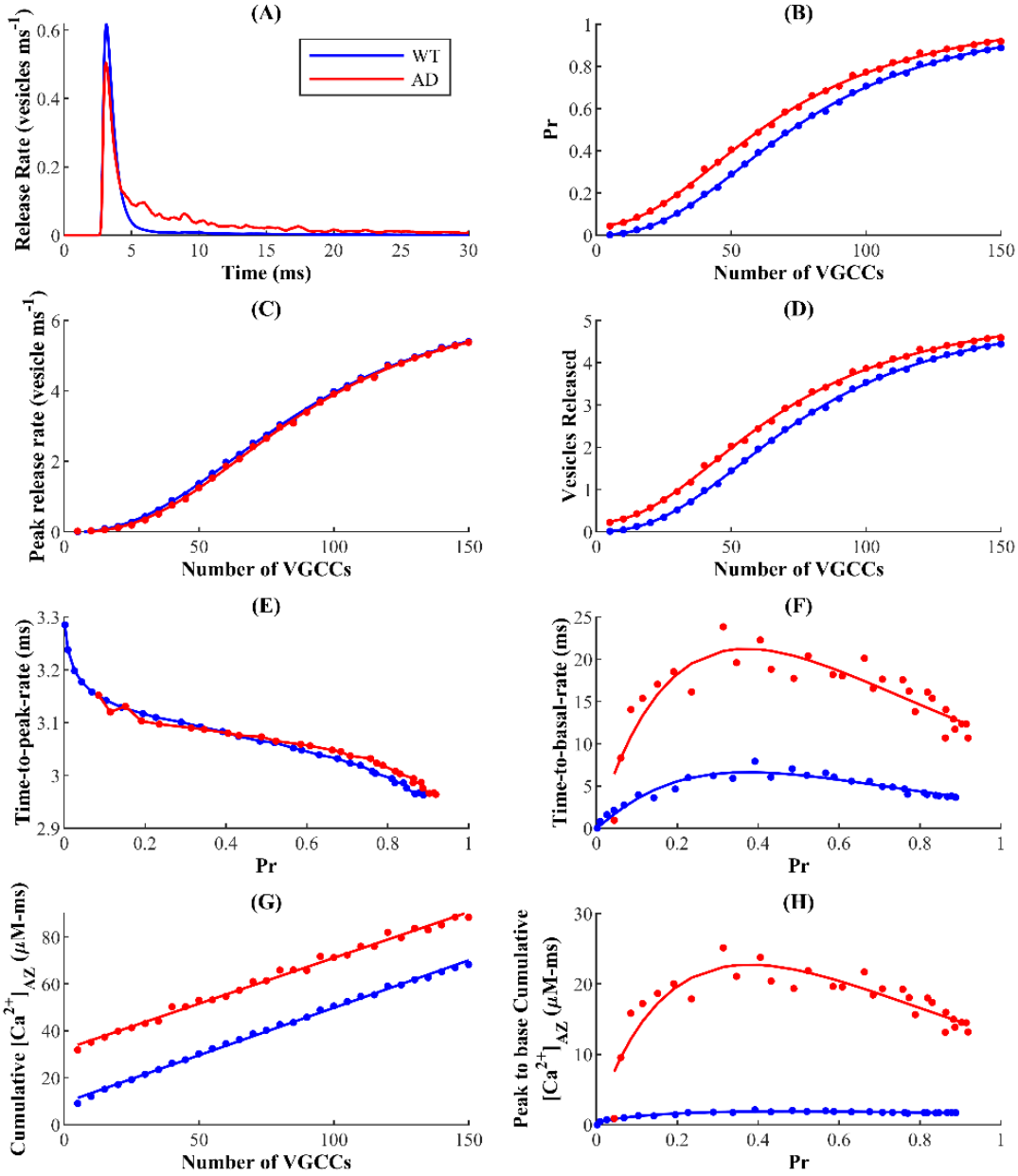

Figure 3. *ER-driven upregulation of cytosolic Ca^{2+} leads to enhanced synaptic vesicle release in AD.* (A) Neurotransmitter release rate in response to a single AP in WT and AD-affected synapse. Change in the Pr of a single synaptic vesicle (B), peak release rate (C), and the average number of vesicles released (D) as functions of the number of VGCCs. (E) Time delay of peak release rate and (F) decay time to basal release rate as functions of Pr. (G) Change in $[Ca^{2+}]_{AZ}$ with number of VGCCs. (H) Cumulative Ca^{2+} from peak to basal level as a function of Pr.

Very short-term plasticity is enhanced in the AD-affected synapse

Next, we investigate how the enhanced Ca^{2+} release from the ER affects very short-term presynaptic plasticity (STP). STP is assessed by determining the paired-pulse ratio (PPR): a classical measure of presynaptic modulation in response to paired stimuli separated by very short time interval [23]. After stimulating the nerve terminal with two pulses separated by a 40 ms interval (*Fig 4A*), we define PPR as the ratio of the Pr following the second pulse (Pr_2) to that of the first pulse (Pr_1) averaged over several trials. Therefore, the response to the second stimulus can either be enhanced with $Pr_2/Pr_1 > 1$ (short-term facilitation (STF)) or depressed with $Pr_2/Pr_1 < 1$ (short-term depression (STD)).

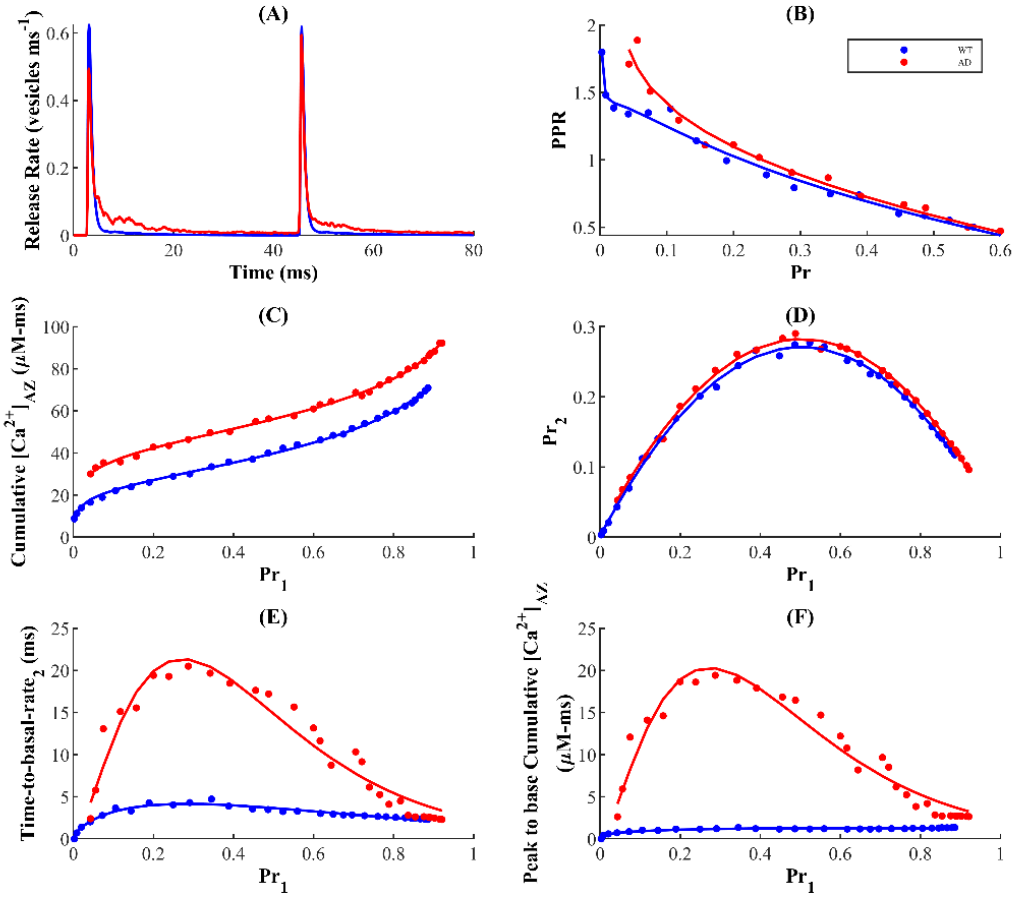

Figure 4. *AD-associated Ca^{2+} upregulation enhances STF*. (A) Release profile following paired-pulse stimulation protocol. (B) PPR is inversely related to intrinsic Pr (obtained after first pulse), and is higher in the AD-affected synapse. (C) Similar to the first pulse (Figure 3G), cumulative $[Ca^{2+}]_{AZ}$ after the second pulse increases with the Pr and is higher in AD-affected synapse. (D) Pr in response to the second pulse (Pr_2) as a function of Pr following the first

pulse (Pr_1). Higher values indicate that the synapse responds more strongly to the subsequent stimulus in a paired-pulse protocol. (E) Decay time of release rate after second pulse also exhibits a biphasic behaviour. (F) Cumulative $[Ca^{2+}]_{AZ}$ following the second pulse reflects the biphasic behaviour observed in time delay of peak-to-basal release rate in panel E.

On average, both WT and AD-affected synapses exhibited an inverse relationship between Pr_1 and the PPR, consistent with previous findings in phasic synapses such as small glutamatergic synapses in the hippocampus *(Fig 4B)* [9, 24, 25, 30]. This negative correlation, thought to be a universal feature of these synapses, is assumed to be caused by the spike-driven depletion of vesicles in the RRP after the first pulse which is unlikely to be recovered by Ca^{2+}-driven facilitation upon the next stimulation. Therefore, whether a synapse exhibits STF or STD is largely dependent on the recent activation history, which implies that synapses with large number of VGCCs and consequently very high intrinsic release probabilities tend to depress their response more severely to a second pulse, allowing them to operate at low PPR [9, 23—26, 29, 30].

While additional mechanisms may contribute to STD, the depletion model of depression in phasic synapses suggests that at rest, the priming sites containing the RRP of vesicles is mostly occupied and reflects the inability of residual Ca^{2+}—left over from the previous stimulation—and the incoming flux to potentiate release during the second stimulation [27, 28]. In agreement with these findings, our model establishes the dynamic equilibrium between the RRP (primed pool) and the unprimed pool by ensuring a relatively faster priming rate. As a result, we find here that most synapses operating in the intermediate-release-probability regime, characteristic of hippocampal excitatory synapses, display low STD with PPR<1 in both WT and disease states *(Fig 4B)*. Strikingly, AD-affected synapse displays enhanced presynaptic strength relative to WT synapse, in contrast to the notion that the activity-dependent tunability of PPR ensures that periods of elevated activity results in subsequently depressed response. A simple explanation for this is that in the AD-affected synapse, the elevated residual Ca^{2+} in the nerve terminal after the conditioning stimulus is longer-lasting and facilitates additional release upon subsequent stimulation *(Fig 4A)*. To test the veracity of this claim, we examined whether the $[Ca^{2+}]_{AZ}$ remains elevated following the second pulse. Consequently, we find that the AD-associated enhancement of residual $[Ca^{2+}]_{AZ}$ is sustained after the second stimulation and increases with Pr_1 *(Fig 4C)*. These results suggest that on short timescales, the reduced

depression observed in AD synapses is orchestrated by Ca^{2+} released from internal stores and induces a history-dependent enhancement of STP with respect to the WT synapse.

Although our results suggest that higher-probability synapses always express greater depression, it is still unclear whether probability of transmission of consecutive spikes monotonically relates to intrinsic release probability, and what role the ER plays in sculpting the concomitant profile. For this purpose, we examine the Pr_2 as a function of Pr_1 *(Fig 4D),* which reflects the conditional probability that a successful release event on the first pulse is followed by another successful release on the second pulse. Our data reveal that the success of a transmission event in response to the second stimulus depends on that for the first stimulus in a bell-shaped manner, indicating that the probability of vesicle release upon consecutive spikes is attenuated at both low and high probability synapses. This implies that synapses with intermediate synaptic transmission failures display higher success of transmission of consecutive spikes, in agreement with the idea that the stochasticity/unreliability of transmission probability can enhance the efficacy of information transmission across the synapse [31—33]. Unsurprisingly, the AD-affected synapse facilitates transmission in response to the second stimulus more strongly compared to the WT synapse. This suggests that diseased synapses retain longer history of Ca^{2+} events, which consequently contributes to hyperactivation of release at short time scales. To verify this claim, we examined whether the biphasic response of the of decay time and cumulative $[Ca^{2+}]_{AZ}$ due to the first stimulus is sustained after the second stimulus. Indeed, we observe that both decay time and cumulative $[Ca^{2+}]_{AZ}$ retain their bell-shaped dependence on Pr_1 *(Fig 4E & 4F)*. Importantly, the AD-affected synapse exhibits markedly enhanced response to the second stimulus following the elevated residual $[Ca^{2+}]_{AZ}$ due to the first pulse, in agreement with the notion that AD-affected synapses can result in enhanced excitation of neuronal processes. These findings are consistent with previous work showing that, particularly in the early stages of AD, over-excitation dominates neuronal circuits with soluble Aβ oligomers and contribute to cognitive dysfunction and impairments [34—36]. In summary, AD-associated enhanced Ca^{2+} release from intracellular stores leads to a history-dependent enhanced STP and hyperactivation of neuronal processes at short time scales with respect to WT synapses. We also notice that the higher coupling strength between the AZ and microdomain of IP_3Rs cluster exacerbate the enhanced PPR but has a marginal effect on the bell-shaped behaviour of Pr_2 as a function of Pr_1 in AD-affected synapses (*Supplementary Fig 2*).

AD-associated Ca^{2+} rises differentially regulate synchronous and asynchronous release during repetitive stimulation

Next, we investigate the effect of upregulate cytosolic Ca^{2+} on synaptic response following trains of stimuli. As in the previous section, we stimulate the synapse with a train of 20 APs delivered at 20 Hz and defined facilitation as the ratio of response following the n^{th} stimulus (R_n) to that of the first (R_1) averaged over several trials. Therefore, synaptic response to successive stimuli in the pulse train can either be depressed, with $R_n/R_1 < 1$, or facilitated, with $R_n/R_1 > 1$. In both WT and AD-affected synapses, repetitive activation leads to depression of both peak release rate (*Fig 5a*) and Pr (*Fig 5b*) that increase with subsequent stimuli. Here, the AD-affected synapse exhibits lower peak release rate (*Fig. 5C*) and baseline Pr (*Fig. 5D*) leading to lower facilitation that persists throughout activation. The depression due to higher-frequency longer (~450 msec) stimulus train observed in the AD-affected synapse results from rapid depletion of the vesicles in the RRP relative to the WT synapse *(Fig 5E)*.

Although evoked peak release rate and Pr exhibit similar decay as functions of pulse number, AD-associated Ca^{2+} disruptions differentially affect these two properties. While the peak release rate in case of the WT synapse remains mostly higher than that of the AD-affected synapse, the Pr in case of AD-affected synapse is consistently higher following successive stimuli (*Fig 5C & 5D*). These results indicate that during ongoing activity, ER-mediated Ca^{2+} disruptions drives a competition between the primary modes of exocytosis; short-lived synchronous release that dominates evoked release during low-frequency stimulation, and slower asynchronous release which persists for several milliseconds and builds up during higher-frequency stimuli trains [1, 37]. Consistent with previous reports, we observe that during the pulse-train depression, synchronous release progressively declines, whereas asynchronous release peaks and subsequently decays with stimulus number (*Fig 5G & 5H*). These results also show that while both forms of release compete for the same pool of releasable vesicles, residual Ca^{2+}, which builds up during repetitive stimulation may allow asynchronous release access to a larger subset of the RRP initially [38, 39, 40]. Our findings here indicate that impairments such as AD pathology, which trigger elevated levels of residual intracellular [Ca^{2+}] (*Fig 5F*), significantly enhance asynchronous release during first few pulses (*Fig 5G*). For both WT and AD-affected synapses, the decrease in asynchronous release after the peak is dictated by competition with synchronous release for the same vesicle resources, which are rapidly depleted with subsequent stimuli (*Fig 5G & 5H*) [39, 41]. Interestingly, the greater

382 degree of depression in the AD-affected synapse is positively correlated with profound increase
383 and decrease in the rates of asynchronous and synchronous release respectively. Together, our
384 data suggest that during the stimulus train, AD pathology elicits significantly more
385 asynchronous release at the expense of synchronous release, consistent with the notion that
386 elevated residual Ca^{2+} underlies asynchronous release. Since the majority of evoked exocytosis
387 occurs synchronously with AP-triggered Ca^{2+} influx, the enhanced switch from synchronous
388 to asynchronous release in the AD-affected synapse reflects the increased depression of
389 synaptic transmission with repetitive stimulation. As clear from *Supplementary Fig 3*, the
390 higher coupling between the microdomain around IP_3Rs cluster and AZ exacerbate the synaptic
391 depression in AD-affected synapses more than WT synapses.
392

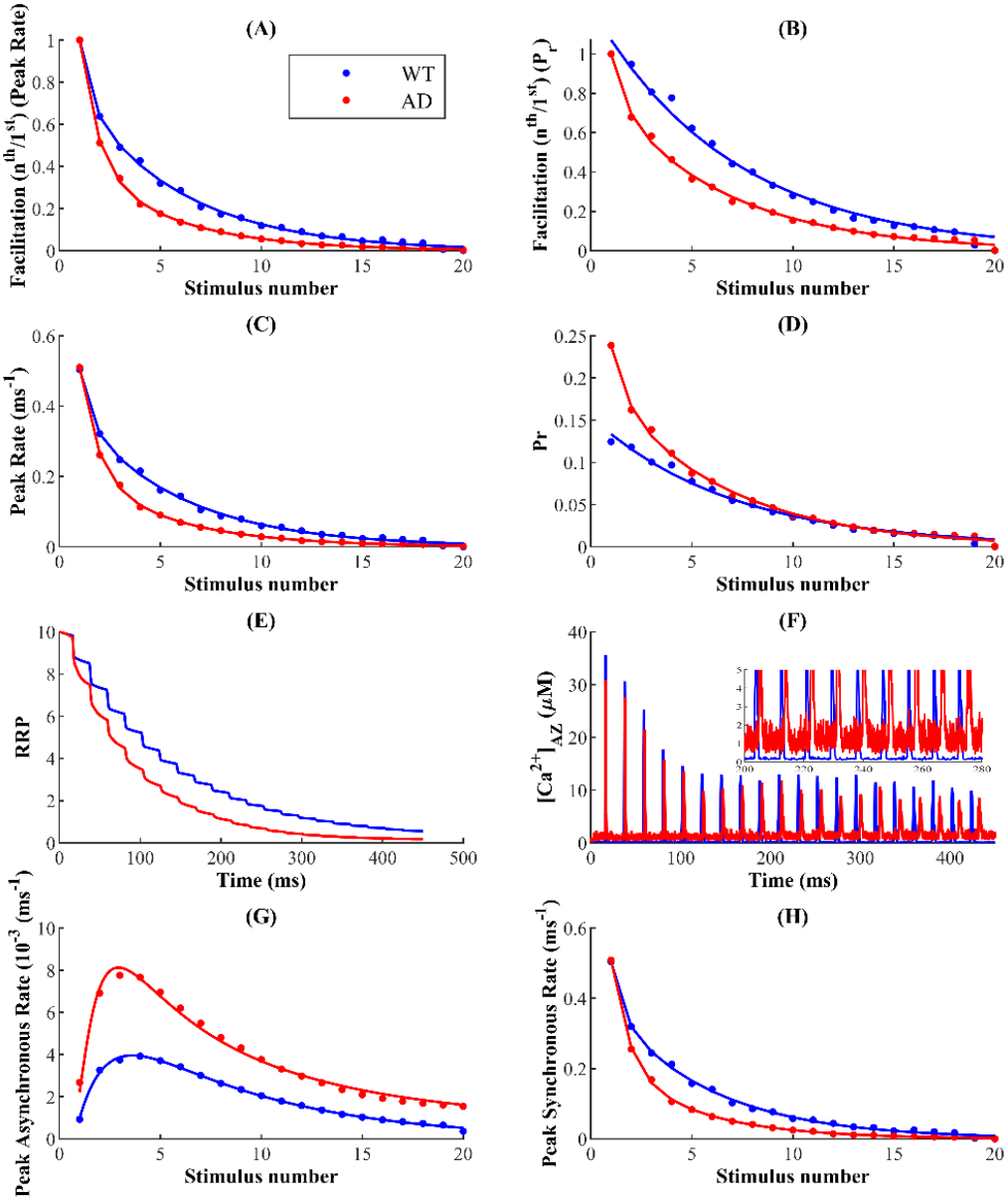

Figure 5. *The AD-affected synapse exhibit stronger depression in response to 20 pulse stimulus-train delivered at 20 Hz*. Facilitation obtained from peak rate (A) and Pr (B) shows that AD pathology induces more severe depression relative to control conditions. Peak release rate (C) and Pr (D) following each AP in the train. (E) Pulse train depression is primarily governed by RRP depletion, which is more severe in synapses with AD pathology. (F) $[Ca^{2+}]_{AZ}$ (top) and zoom-in (inset) showing the differences in basal $[Ca^{2+}]_{AZ}$ levels. (G) Asynchronous release peaks and subsequently decays following depletion of RRP. (H) Peak synchronous release mimics the response seen in the overall release.

Synchrony of release events is reduced in the AD-affected synapses

Motivated by substantial evidence supporting reduced temporal coordination of neural activity in AD-affected networks, we next examine the degree of synchronization between stimulus and response in WT and AD-affected synapses during repetitive stimulation [118—120]. Given the loose temporal coordination of neuronal response during asynchronous release, the observed shift from synchronous to asynchronous release during stimulation in AD should reduce the synchrony between the pulse and response [39]. To test this hypothesis, we measure the event synchrony between each spike in the pulse train and corresponding release using a modified Pinsky-Rinzel algorithm (see Methods for details) [121, 123]. In extreme cases, pulse and release event times can either be perfectly aligned with synchrony value of 1, reflecting pristine temporal stimulus-response coordination, or desynchronized where synchrony value of 0 reflects temporally uncorrelated activity and stimulus patterns.

The phase of individual release events in response a stimulus train reveals that synapses with AD pathology exhibit significant decrease in coherence of stimulus and release events, an observation that is seen consistently across a wide range of the Pr values (*Fig 6a & b*). In-silico studies of the effect of presynaptic Ca^{2+} stores on exocytosis at the CA3 terminal suggest that the ER allows highly stochastic hippocampal synapses with low intrinsic release probability to operate with increased reliability [9]. Unsurprisingly, in both the diseased and WT cases, synapses with low Pr exhibit relatively higher phase coherence that persists upon subsequent stimulation (*Fig 6a & b*). Thus, our findings here suggest that the alternative strategy to achieve robust firing rates—employed by synapses with high intrinsic Pr that deplete the RRP quickly—may render the synapses unreliable during repetitive stimulation.

Furthermore, a quantitative comparison of the synchrony measure reveals that AD-affected synapses with altered intracellular Ca^{2+} signalling exhibit significantly reduced temporal coordination of activity as compared to WT synapses. This suggests that in addition to other impairments discussed above, unreliability in the temporal coordination of neuronal activity is also a key hallmark of AD-affected synaptic terminals (*Fig 6c*). This conclusion is consistent with *in vivo* recordings from neocortical pyramidal neurons where amyloid-β plaques in APP-Sw (Tg2576 transgenic mice model of AD) increased jitter in evoked AP, consequently reducing synaptic integration and information transfer [122]. Although our data so far indicate

that synapses with higher Pr express reduced synchronization in both WT and AD conditions, the relative sensitivity of synapses with low, intermediate, and high Pr to pathological alternations is yet to be explored. Thus, we next examine the relative change in synchrony from WT to AD condition across a wide range of Pr values (*Fig 6d*). Our results show that there is an inverted bell-shaped relationship between relative synchrony and intrinsic Pr, suggesting that the physiological (intermediate) Pr which allows small hippocampal synapses to operate with reliable firing rates also renders them more sensitive to pathological alterations. Taken together, these data suggest that the pathophysiological manifestations of impaired intracellular Ca^{2+} handling include suboptimal neuronal synchronization, reducing the fidelity of information integration and transmission. In addition, the results confirm that hippocampal synapses with intermediate Pr values exhibit a more severe impairment of their otherwise finely tuned temporal rate codes when subject to AD-related alterations in Ca^{2+} signalling.

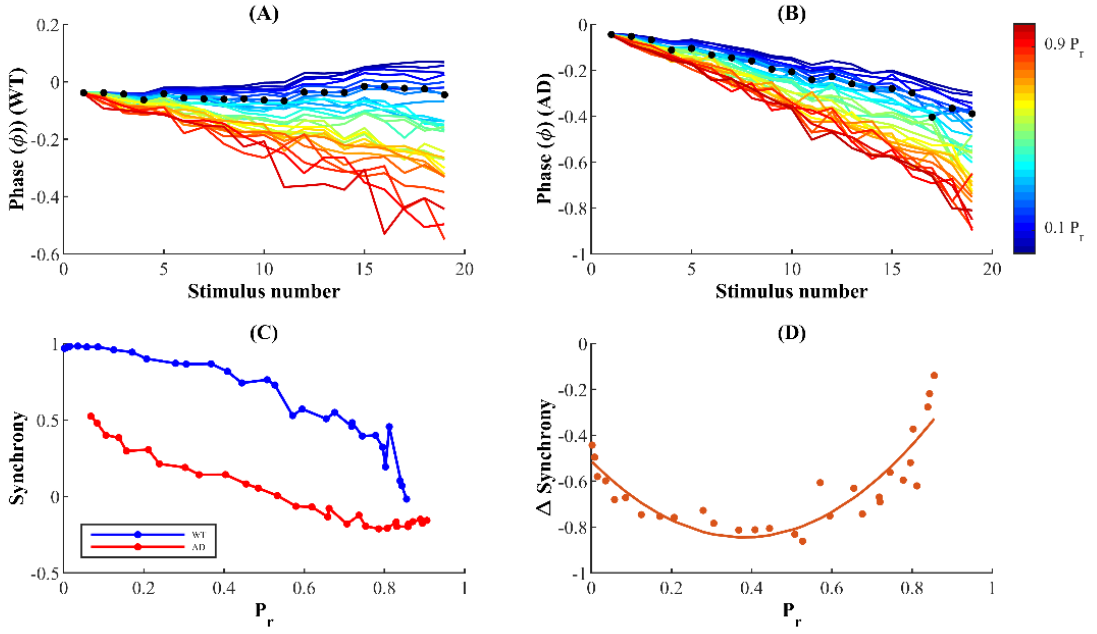

Figure 6. *AD-related Ca^{2+} disruptions impair spike-SVR synchrony*. The phase of individual release events with respect to AP in WT (A) and AD-affected (B) synapses over a wide range of Pr values. Black dots indicate the event phases corresponding to 35 VGCCs with initial Pr during pulse train (Pr_1) equal to 0.14. (c) Synchrony of release event in response to the preceding pulse in WT and AD-affected synapses. (d) The magnitude of relative synchrony change from WT to AD conditions as a function of initial release probability during prolonged stimulation.

Discussion

Despite extensive experimental studies reporting the ubiquitous presence of ER in both axonal and dendritic compartments of neurons, little is known about its role in modifying major components of synaptic transmission during AD related pathologies [42–44]. In this study, we fill this gap by building a detailed biophysical model that accurately captures the compartmentalized signalling of Ca^{2+} at axonal terminals. In particular, our model incorporates ER-driven and AP-triggered presynaptic Ca^{2+} signalling as well as the resulting release mechanism in WT and AD-affected synapses. This is especially motivated by reports of distinct regulatory mechanisms for intracellular Ca^{2+}, which primarily includes a cluster of ligand-gated IP_3R Ca^{2+} channels situated on the ER as well as voltage activated Ca^{2+} channels constrained to the AZ, that result in tight microdomain signalling [6, 66—69]. In hippocampal synapses, the formation of evoked transient Ca^{2+} microdomains in the AZ is predominantly mediated by the rapid kinetics of P/Q-type VGCCs which open with minimal delay upon the arrival of AP, while subcellular domains in the vicinity of the ER occurs via the stochastic gating of IP_3Rs that require IP_3 and Ca^{2+} binding. In order to make meaningful quantitative predictions, we proceeded by developing a model that accurately captures the characteristic IP_3R's gating in WT and AD-affected neurons [16, 17, 128]. We next, incorporated a comprehensive description of presynaptic processes including evoked Ca^{2+} influx through VGCCs; Ca^{2+} release and uptake by the ER; and synchronous, asynchronous, and spontaneous modes of synaptic transmission. Inspired by several lines of evidence elucidating the existence of a bidirectional interaction of intracellular Ca^{2+} channels and presynaptic VGCCs mediated by stromal interaction molecules (STIM-1) and Orai channels, we have implemented a bi-directional coupling between the ER and AZ in our model that uncovers a unique biphasic dependence of decay times of release and Ca^{2+} on the baseline probability [7, 73]. Our model incorporates these critical components of presynaptic signalling and especially reproduced the observed spatiotemporal characteristics of intracellular Ca^{2+}—rise times, decay times, and amplitudes of corresponding events—and accounts for the stochasticity of presynaptic Ca^{2+} dynamics driven by stochastic channel openings [6, 16, 70, 71]. Release rate, facilitation and depression varies dramatically among phasic and tonic synapses—phasic synapses are dominated by depression, whereas tonic synapses can facilitate tremendously by vesicle recruitment [27, 28]. Constrained by kinetics data of vesicular release observed in other phasic

cell types, our model closely reproduces essential determinants of neurotransmitter release, which consequently promoted close estimation of PPR and facilitation requirements necessary to maintain normal plasma membrane function [23, 24, 28]. Following these independent validations, it is reasonable to assume that the biophysical model and protocols developed in this work are physiologically realistic representation of neuronal processes in control and disease cases.

Broadening of Ca^{2+} waveforms and response profiles affect the reliability of synaptic information transfer at affected terminals. Our results suggest that AD-associated increase in Ca^{2+} release from the ER affect nearly all aspects of SVR. Despite the high stochasticity at the hippocampal CA3 terminal, the ER allows individual synapses operating in the low- and intermediate-probability regime maintain relatively higher reliability of information-rate coding [9]. Here, our results show that the AD-associated enhanced Ca^{2+} selectively diminishes the reliability of intermediate-Pr synapses, suggesting that low- and intermediate Pr synapses are more susceptible to AD-associated Ca^{2+} disruptions. Importantly, the model predicts that aberrant Ca^{2+} rise in AD-affected neurons may trigger hyperactivity over very short timescales (~30-60 msec) and lowers facilitation during prolonged (~450 msec) stimulation. We also report enhanced excitability in pathological synapses when simulated with higher coupling, which corresponds to a tighter feedback loop between the ER and AZ. Thus, our findings here provide a plausible explanation for why alterations in ER Ca^{2+} handling, which result in excessive efflux, induce a severe perturbation of neuronal processes that can in turn decrease the reliability of information encoded in the firing rate of neurons affected by AD pathology [9, 72]. Overall, our findings provide novel insights into the role of aberrant ER Ca^{2+} release in altering the release profile of a synapse in AD and other neurodegenerative diseases where such Ca^{2+} impairments are observed [136].

Many explorations into the Ca^{2+}-dependence of release have proposed that periodic Ca^{2+} release from the ER, which occurs predominantly via the rapid gating kinetics of IP_3R, could trigger a series of physiological events—such as activating Ca^{2+}-sensing G proteins—that eventually manifest as changes in the global $[Ca^{2+}]$ and, in turn, influence spontaneous release: a miniature form of exocytosis [21, 47]. Although IP_3Rs are differentially expressed according to cell type, several studies report the functional involvement of IP_3Rs in sculpting long-term potentiation (LTP) or depression (LTD) profiles in the CA1 region of the hippocampus [48, 50]. In particular, immunocytochemical evidence reveals the expression of IP_3Rs in presynaptic

terminals of the rat CA3-CA1 hippocampal synapses and elucidates their modulatory role in presynaptic neurotransmitter release and synaptic plasticity [49]. Shorter opening times and longer closing times are characteristic features of the gating kinetics of IP_3Rs in cortical neurons and are essential for the homeostasis of local and global Ca^{2+} in the norm. Consistent with these requirements, studies on AD patients have implicated exaggerated Ca^{2+} release mediated by altered IP_3R activity to dysregulation of bulk Ca^{2+} which consequently triggers progressive loss of synaptic function [51—54]. From our model it is clear that these intrinsic biophysical properties of IP_3R make it highly effective at maintaining physiological bulk Ca^{2+} and *Pr,* whereas upregulated IP_3R orchestrates exaggerated Ca^{2+} from the ER and in turn increases the Pr.

Consistent with experimental evidence, our model reproduces the well-established inverse relationship between the Pr and PPR but suggests that the enhanced STP over rapid timescales observed in AD merely indicates hyperactivity rather than increased synaptic reliability [23, 59]. The most crucial insight from this finding is that pathological synapses retain a longer history of Ca^{2+} dynamics, which consequently causes them to exhibit enhanced excitation in a paired-pulse protocol. The traditional view claiming the massive reduction in the efficacy of excitatory synaptic transmission in early stages of AD has been challenged recently by several studies reporting aberrant Ca^{2+} homeostasis and hyperactivity in AD-affected neuronal networks [10, 36, 34]. A key finding of these studies is that hyperactivity is an early dysfunction in hippocampal synapses, whereas neuronal silencing emerges during later stages of the disease. Our model predicts that synaptic facilitation and depression depend on the timescale and frequency of stimulation. Relatively short low-frequency stimuli cause facilitation, which supports the idea that by enhancing potentiating over rapid time scales, aberrant Ca^{2+} release from intracellular stores plays an important role in the history-dependent neuronal hyperactivity observed during early states of AD.

Our model shows that long high-frequency pulses trigger depression in AD-affected synapses, which is governed by depletion of RRP of vesicles. Experimental evidence reports three distinct molecular pathways for exocytosis [37]. Indeed, synchronous, asynchronous, and spontaneous modes of vesicular release, characterized by distinct release timescales, have been reported in cultured hippocampal synaptic terminals [21, 38]. Synaptotagmin-1 (Syt1) and 7 (Syt7) are the Ca^{2+} sensors controlling the timescales of synchronous and asynchronous release in CA3 pyramidal neurons respectively [37, 60]. The rapid kinetics and low Ca^{2+} affinity of

Syt1 satisfies the remarkable temporal precision of synchronous release, where most vesicles immediately fuse with the membrane following stimulation. On the other hand, the slow kinetics of Syt7 promotes progressive desynchronization of release later in the spike train [61]. Studies on Syt1 knockout mice reported selective abolishment of synchronous release and increase in the magnitude of asynchronous release. Likewise, knockdown of Syt7 enhanced synchronous release in zebrafish's neuromuscular junction, suggesting that the primary modes of exocytosis draw from the same vesicle resources in the RRP, which causes their activity patterns to be negatively correlated [38, 61—65]. The most critical insight of these findings is that manipulations that supress synchronous release increases the vesicle resources available for asynchronous release and indirectly enhance its magnitude. In agreement with the above, during ongoing activity, we observed a shift from synchronous to asynchronous exocytosis leading to increased depression of synaptic transmission during AD pathology.

CA3-CA1 presynaptic terminals are equipped with a conspicuously low release probability that allows them to maintain a delicate balance between facilitation and reliability, giving rise to finely tuned rate codes with remarkable temporal precision. Thus, perturbations of release mechanisms are expected to alter the fidelity of neural rhythms in AD. Indeed, cortical neurons with Aβ peptide expressed reduced N-methyl D-aspartate (NMDA) receptor density, resulting in rapid and persistent depression of NMDA-evoked currents [120]. Moreover, the severe impairment of evoked synaptic response latency observed in Tg2576 mice overexpressing APP provides direct evidence for reduced temporal coincidence of response in AD [122]. These findings suggest that impaired response precision is an acute effect of perturbations due to AD that leads to overt cortical deficits. In agreement with these observations, our results reveal increased latency of release events in AD and uncover unique dependence of synchrony change—from control to AD—on intrinsic Pr. The loss in temporal coordination of release in AD is more severely expressed at a physiologically plausible Pr range for hippocampal synapses, although lower-Pr synapses exhibit relatively elevated temporal precision in both WT and AD-affected synapses. Thus, despite the high fidelity of hippocampal synapses, their conspicuously low response success may make them more susceptible to AD pathology. We hope that future experiments will uncover the molecular mechanisms underlying the pathological enhancement of susceptibility in low-Pr hippocampal synapses.

We remark that while our model is developed to be consistent with most observations in the hippocampal CA3-CA1 synapses, it does not incorporate the uneven distribution of P/Q-type,

N-type and R-type VGCCs specifically found in the AZ of central synapses [74, 75]. At hippocampal glutamatergic synapses, Cav2.1—P/Q-type—channels are thought to be most enriched at the presynaptic AZ and predominantly govern Ca^{2+} influx at the axon terminal [78]. Thus, like others, we value parsimony and use a formulation with only P/Q VGCCs [70]. Furthermore, results from cultured hippocampal and superior cervical ganglion neurons provide evidence for direct interactions between the release machinery and VGCCs, implying that channel distribution is important for accurately predicting the spatiotemporal profiles of evoked release [76, 77]. Our model does not capture the effect of spatial distribution of VGCCs on synaptic transmission, neither does it incorporate other mechanisms for paired-pulse modulation expressed at putative single hippocampal synapses—lateral inhibition and release inactivation [23, 24]. Thus, despite reproducing the observed inverse relationship between paired-pulse facilitation and initial Pr, our model falls short of the measured values, suggesting that we cannot eliminate additional mechanisms when investigating the interplay between residual Ca^{2+}, facilitation, and depression. Although IP_3R-dependent modulation of cytosolic Ca^{2+} is usually adequate for explaining the critical aspects of ER Ca^{2+} release and regulation of neurotransmission, the upregulation of RyR expression and modulation of IP_3Rs' gating due to Ca^{2+} release through RyRs (and vice versa) are also thought to play a key role in the aberrant Ca^{2+} release from the ER, as well as propagation of presynaptic signals [16, 17, 79, 94—100, 127—129]. It has been suggested that at the hippocampal Schaffer-collateral pathway, presynaptic presenilin inactivation perturbs STP and facilitation via impaired RyR function [80, 81]. Furthermore, in 3xTg-AD mice, deviant RyR activity triggers Ca^{2+} signalling alterations that promote synaptic depression [82]. However, our model does not describe the contribution of presynaptic RyRs to vesicular release, as the biophysical properties of these receptors yield a distinct temporal range of Ca^{2+} transients that can modulate LTP/LTD [83, 84]. Another key factor missing from our model is synaptic mitochondria. Mitochondria play a key role in shaping Ca^{2+} gradients in synaptic terminals. Synaptic mitochondria are among the earliest targets in AD. Among other things, the ATP production and Ca^{2+} buffering capacities of mitochondria are severely disrupted [140, 141]. All these issues are the subjects of our future research.

In summary, we have leveraged diverse experimental data to model Ca^{2+} homeostasis in axonal terminal and how exocytosis is affected in AD. Motivated by the difficulty in probing signalling cascades at the AZ of small hippocampal synapses, our main goal was to build a comprehensive but simple framework for unravelling the role of enhanced Ca^{2+} release from the ER in SVR

during AD pathology. In addition to agreeing closely with several observations about the kinetics of IP_3Rs, SVR, and synaptic plasticity in both WT and diseased synapses, our modelling work provides key insights into impaired presynaptic function in AD. Specifically, we make five key predictions: (1) the overall Pr in response to a single AP is upregulated in AD-affected synapses, (2) short-lived low-frequency stimuli promotes potentiation in AD-affected synapses, (3) during sustained high-frequency stimulation, AD-affected terminals exhibit enhanced depression, (4) AD-affected synapses operate less reliably, and (5) the effect of AD pathology is exacerbated in synapses with low to intermediate Pr. Taken together with the aforementioned limitations, our analysis highlights the need for further studies on investigating the role of perturbed Ca^{2+} signalling due to intracellular organelles such as the ER and mitochondria in cognitive deficits associated with AD and other neurodegenerative diseases.

Materials and Methods

Calcium model

Building on extensive literature, we capture intracellular Ca^{2+} dynamics by first developing a compartmental model of a hippocampal CA3 axonal bouton, which includes main fluxes that invade the bulk cytosol as well as regulatory mechanisms present in the ER [67, 109—111] (*Fig. 7*). Our canonical synaptic bouton is modelled as a sphere with fixed volume V_{bouton} = 0.122 μm^3, in agreement with findings from ultrastcutural analysis of hippocampal synapses [2, 78]. We consider an average of 1.3 AZs in small hippocampal boutons implemented in a spherical AZ (with area = 0.04 μm^2) [2, 78]. Although we assume a well-mixed cytoplasm, we next incorporate two microdomains of sharp Ca^{2+} transients produced by clusters of IP_3R and VGCCs proximal to the ER and plasma membrane respectively. Because the VGCCs (P/Q-type Cav2.1 channels) implemented here are spatially distributed in small clusters within the AZ, we implemented a characteristic 25 nm cluster [6, 78]. To account for the spatial extent of the Ca^{2+} domain in the vicinity of the VGCCs cluster, we use the findings in cortical pyramidal terminals that show that low mM concentrations of the slow Ca^{2+} buffer ethylene glycol tetraacetic acid potently attenuates transmitter release [46, 115, 116] for guidance. We consider a cytosol-to-VGCCs microdomain ratio of 60, assuming a domain of elevated [Ca^{2+}] that extends over more than 100 nm [46, 66]. As a result of these considerations, the Ca^{2+} dynamics

in the respective compartments as well as the entire bouton ($[Ca^{2+}_{total}]$) is described by four couple non-linear ODEs (*Eqs. 1-4)*. *Tables 1* defines the fluxes (J) in terms of various Ca^{2+} concentrations, along with volume fractions. The parameters used are listed in *Tables 2* and *3*. As a critical second messenger, the pathways for IP_3 metabolism are succinctly described in *Eq. 5* [112, 114], with further details in *Table 4*. Inhomogeneity of ligands persists throughout the bouton; however, we assume spatially homogenous compartments, and only track temporal evolution of ligands.

$$\frac{d}{dt}[Ca^{2+}_{cyt}] = J_{in} + J_{IPR-diff} - J_{PMCA} + J_{ER-leak} + J_{VGCC-diff} - J_{SERCA}, \quad (1)$$

$$\frac{d}{dt}[Ca^{2+}_{IPR_n}] = \delta_1\left(J_{IPR} - J_{IPR-diff}\right) + J_{coupling}, \quad (2)$$

$$\frac{d}{dt}[Ca^{2+}_{AZ}] = \delta_3\left(J_{VGCC} - J_{VGCC-diff}\right) - \frac{1}{\delta_1}J_{coupling}, \quad (3)$$

$$\frac{d}{dt}[Ca^{2+}_{total}] = J_{in} - J_{PMCA} + J_{VGCC}\ , \quad (4)$$

$$\frac{d}{dt}[IP_3] = \frac{1}{\tau_{IP_3}}(J_{PLC} - J_{deg})\ , \quad (5)$$

where $[Ca^{2+}_{cyt}]$ is the Ca^{2+} concentration in the cytosol, $[Ca^{2+}_{IPR_n}]$ is the Ca^{2+} concentration in the microdomain surrounding the IP_3Rs, and $[Ca^{2+}_{AZ}]$ represents the Ca^{2+} concentration surrounding the small cluster of VGCCs in the AZ.

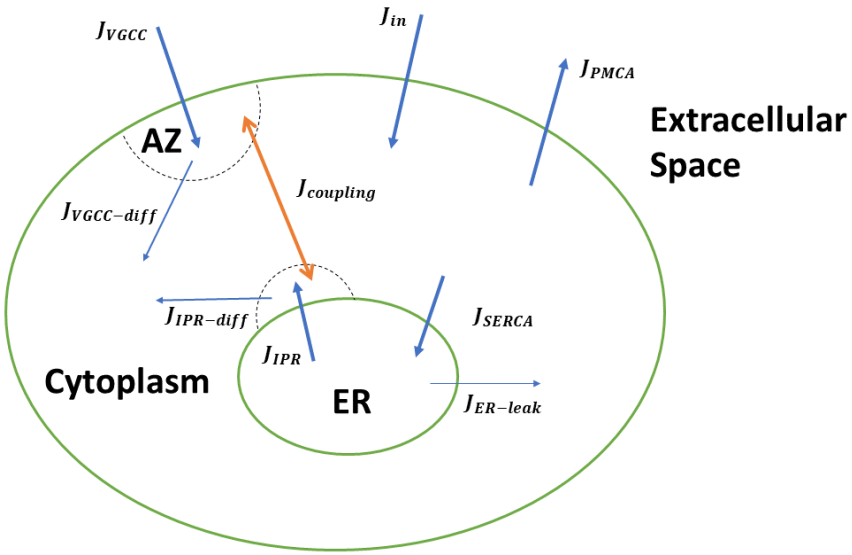

Figure 7. *Schematic of the overall multi-compartmental Ca^{2+} model***.** The arrowheads show the direction of the fluxes involved and the dotted half circles signify the Ca^{2+} domains around the IP_3Rs and VGCCS clusters.

The Ca^{2+} concentration in the ER is given by $[Ca_{ER}^{2+}] = \delta_2\left(Ca_{total}^{2+} - Ca_{cyt}^{2+} + Ca_{IPR_n}^{2+}/\delta_1 - Ca_{AZ}^{2+}\right)$. δ_1, δ_2, and δ_3 represent the volume ratios of the intracellular compartments and are explained in *Table 4*. Fluxes in our model were selected to account for the essential regulating components of intracellular Ca^{2+} signalling. J_{in} represents the Ca^{2+} entry through plasma membrane channels such as store operated Ca^{2+} channels (SOCC) and basal plasma membrane leak. J_{IPR} represents release from the ER through IP_3Rs, whereas Ca^{2+} diffusion from the microdomain around IP_3Rs cluster to the bulk cytosol is modelled by $J_{IPR-diff}$. Likewise, $J_{VGCC-diff}$ and J_{VGCC} are included to account for Ca^{2+} diffusion from the AZ to the bulk cytoplasm and influx through VGCCs respectively. Ca^{2+} efflux from the intracellular compartment by plasma membrane Ca^{2+} ATPase (PMCA) is captured by J_{PMCA}, and $J_{ER-leak}$ is the Ca^{2+} leak from the ER. Sequestering of Ca^{2+} from the cytoplasm into the ER through Sarco/Endoplasmic Reticulum Ca^{2+} ATPase (SERCA) is represented by J_{SERCA}.

To investigate the effect of altered ER Ca^{2+} handling on vesicular fusion situated in the AZ, we incorporate a flux ($J_{coupling}$) intended to mimic the close association of the ER with the nerve terminal of CA3 pyramidal neurons [101—103]. Based on evidence of the existence of a feedback loop between synaptic function and ER Ca^{2+} content, we build a bidirectional model of Ca^{2+} exchange. We assume a simple transfer of Ca^{2+} between the two microdomains, potentially mediated by Ca^{2+} buffering and enzymatic proteins. This coupling is modelled by an equation analogous to bidirectional models of SERCA flux (*Eq. 6)* [111], which where V_c is the maximum flux from the AZ to the microdomain around IP_3R cluster and K_c determines the half-maximal transfer rate.

$$J_{coupling} = V_c \frac{([Ca_{AZ}^{2+}]^2 - \bar{k}([Ca_{IP_3R_n}^{2+}]^2))}{[Ca_{AZ}^{2+}]^2 - {K_c}^2}. \quad (6)$$

There is strong evidence that the expression of Ca^{2+} buffering proteins in AD affected neurons is significantly lower than WT neurons [133—135]. We incorporate these observations in our model by using parameter values that results in a stronger coupling in AD-affected bouton as

compared to WT bouton. Although the choice of the model has its limitations, using a model that captures buffered Ca^{2+} diffusion becomes numerically intractable quickly as distances approach physiologically reasonable order of nanometres. Thus, this approach provides an extremely useful method to account for the interplay of $[Ca^{2+}_{AZ}]$ and $[Ca^{2+}_{IPR_n}]$.

IP$_3$R model

In the past, several models for IP_3Rs have been developed in WT and AD-affected cells [16, 137—139]. All these models are based on data obtained from non-neuronal cells. While these models can be used to make reliable qualitative predictions, our goal here is to quantify the effect of upregulated Ca^{2+} signalling on neurotransmitter release where a small difference in the open probability of the channel or dwell times can result in a significant change due to the small volume of the synaptic terminal. Thus, we developed a new four-state model to implement the kinetics of IP_3Rs (*Fig. 8A*). The channel has zero, two, two, and five Ca^{2+} bound when in the Resting (R), Active (A), Open (O), and Inactive (I) states, respectively. The transition rates between different states and the corresponding parameters are reported in *Tables 5* and *6* respectively. As shown in *Fig. 1*, the model closely fits the kinetics of IP_3R in neurons from WT and 3xTg AD mice observed in [127]. In the cluster, the gating of each IP_3R is regulated by the Ca^{2+} concentration in the microdomain around the cluster.

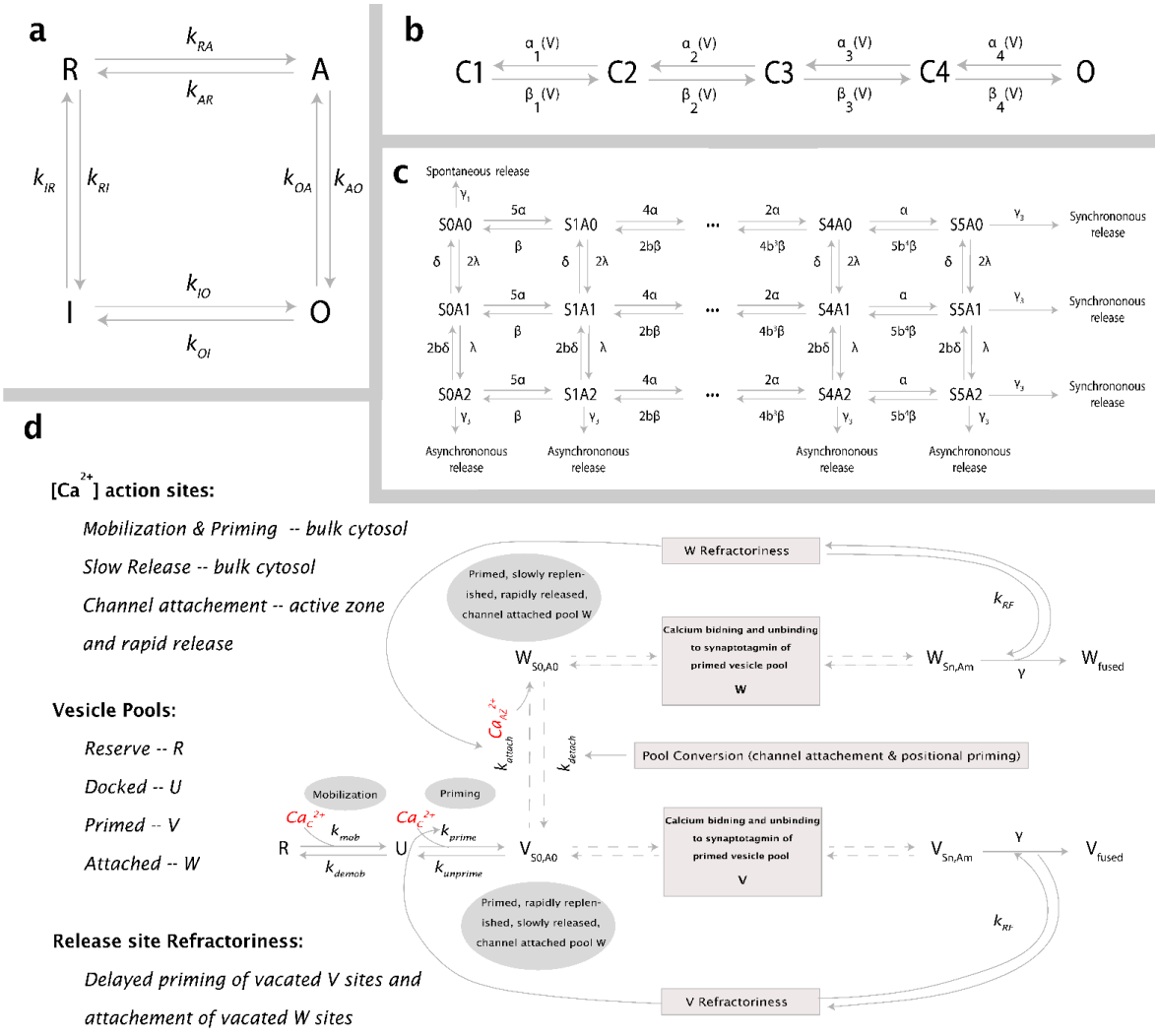

Figure 8. *Kinetic schemes used in the model*. (A) Gating kinetics of IP_3R. Four-state model representing the possible states along with corresponding transition rates. (B) Model for VGCC gating with four closed states (C1 - C4) and one open Ca^{2+} conducting state (O). (C) Scheme for Ca^{2+} binding to Synaptotagmin with dual Ca^{2+}sensors for fast synchronous (S with five Ca^{2+}-binding sites), slow asynchronous (A with two Ca^{2+}-binding sites), and spontaneous exocytosis. (D) Modified from [27], the overall release scheme which includes vesicle mobilization from a reserve pool (R) to docked, unprimed pool (U), molecular priming to vesicles unattached to a Ca^{2+} channel (V), and conversion to vesicles coupled to a VGCCs cluster (W). Both vesicle pools are released through the dual sensor release model. Channel attached vesicles are steeply dependent on $[Ca^{2+}]_{AZ}$, whereas $[Ca^{2+}]_{cyt}$ governs the release of detached vesicles. Reaction rates along with respective references are listed in *Tables 6, 8,* and *9*.

734 ***Membrane voltage dynamics***

735 The basic equations for the membrane potential used in our model are adopted from Ref. [125].
736 Membrane potential (V) is governed by primary Na^+ (I_{Na}), K^+ (I_K), Cl^- (I_{Cl}), and Ca^+ (I_{Ca}),
737 currents, as well as current due applied stimulation (I_{app}), and is given as,

738 $$C_m \frac{dV}{dt} = I_{app} + I_{Na} + I_K + I_{Cl} + \left(\frac{I_{Ca}}{Area}\right),$$

739 where we assumed standard membrane capacitance C_m of $1\mu F/cm^2$. The Na^+ and K^+
740 concentrations were assumed to be fixed, with corresponding currents consisting of active and
741 passive leak components given by

742 $$I_{Na} = -(g_{Na} {m_\infty}^3 h)(V - E_{Na}) - g_{Na_{leak}}(V - E_{Na}),$$

743 $$I_K = -\left(g_K n^4 + \frac{g_{AHP}[Ca^{2+}]_{cyt}}{1+[Ca^{2+}]_{cyt}}\right)(V - E_K) - g_{K_{leak}}(V - E_K).$$

744 Chloride currents only consist of passive leak contribution, defined by $I_{Cl} = -g_{Cl_{leak}}(V -$
745 $E_{cl})$.

746 The steady state gating activation and inactivation variables, as well as associated channel
747 forward and reverse rates were calculated using the equations in *Table 7*. Various parameters
748 used in the membrane potential equations are listed in *Table 8*.

749

750 ***Voltage gated Ca^{2+} channels***

751 Consistent with findings in [75], we implement only the predominant high-threshold Cav2.1
752 (P/Q-type) channels present at presynaptic nerve terminals using a five-state kinetic scheme
753 (see *Fig. 7B*). Voltage-dependent activation and deactivation rates for each closed state (i = 1,
754 2, 3, 4) were respectively calculated as follows: $\alpha_i(V) = \alpha_{i0} exp(V/k_i)$, $\beta_i(V) =$
755 $\beta_{i0} exp(V/k_i)$, where values for activation and deactivation rates at 0 mV, α_{i0} and β_{i0}, and for
756 slope factor k_i were taken from [75] and listed in *Table 8*. As with the IP_3Rs, we model VGCC
757 gating stochastically as a discrete-time Markov Chain (DTMC) (see "*Numerical Methods*"
758 section below). Single channel Ca^{2+} currents were calculated using $I_s = gP_o(V - E_{Ca^{2+}})$,
759 where values for conductance g, extracellular Ca^{2+} concentration and Nernst potential $E_{Ca^{2+}}$
760 were obtained from [6] and are reported in *Table 8*.

Overall release model

The complete release scheme has been adopted and modified from [27] (see *Fig. 7C & 7D*). In addition to the Ca^{2+}—dependent vesicle mobilization and priming steps, we replace the independence of Ca^{2+} binding to C2A and C2B domains of synaptotagmin with the dual sensor model proposed in [1], where two independent Ca^{2+} sensors act in parallel to trigger distinct pathways of exocytosis that lead to fast synchronous, slow asynchronous, and spontaneous release. Synchronous release is mediated by the sensor S with 5 Ca^{2+}-binding sites and cooperativity(b) incorporated to progressively decrease backward rates— Ca^{2+} unbinding. Synchronous fusion occurs when all 5 binding sites are occupied. Likewise, the sensor A— with 2 Ca^{2+}-binding sites—mediates asynchronous release with the same cooperativity parameter b. Spontaneous release is also included and occurs at a much slower rate when the sensors have no Ca^{2+} bound. As in [70], release rates and model parameters were obtained according to fits to experimental data reported in [113]. Contrary to the dual sensor model of [1], we do not assume the synchronous (γ_2) and asynchronous (γ_3) release rates to be the same. This is because according to [70], hippocampal release rates from [113] could not be fitted otherwise. Consequently, we use the release rate for the asynchronous release to be $a\gamma$ where $a = 0.025$.

As described in [1] and shown in *Fig. 2*, compared to the Allosteric model, this model captures the expected heterogeneity and latency of exocytosis more accurately at the Calyx of Held. Apart from the intrinsic heterogeneity of release pathways, the model implemented here captures the heterogeneity of vesicle pools—slow and fast—, where docking and priming are part of the upstream processes for recruiting vesicles into the Slow-Releasing Pool (SRP) and super-priming of vesicles in the SRP aids the conversion of SRP vesicles to those in the Fast-Releasing Pool (FRP). The recruitment of vesicles into the SRP is dependent on the cytosolic $[Ca^{2+}_{cyt}]$, whereas channel attachment is aided by Ca^{2+} influx. As described in *Fig 7*, the target of Ca^{2+} mediating vesicle fusion depends on which pool the fusing vesicle belongs to; for vesicles in the FRP, this is $[Ca^{2+}_{AZ}]$, while those in the SRP bind $[Ca^{2+}_{cyt}]$.

We also include release site refractoriness introduced in [27, 70] in order to simulate experimental observations. In this context, a vesicle cannot be released from a vacated site for

a period determined by k_{RF}, such that sites—either Ca^{2+}-attached (W) or detached (V)—from which vesicles had been released remain unable to accept a new primed vesicle for some time. Phasic synapses are known to have briefer refractoriness compared to their tonic counterparts, and as such, we choose k_{RF} to be $0.01\ ms^{-1}$, similar to values observed at hippocampal synapses in [23]. Different parameters used in the release model are listed in *Table 9*.

Synchrony measure

For a wide range of synaptic configurations with distinct intrinsic release probabilities, we computed the synchrony of AP arrival times (estimated at peak) and release event times using a modified version of the Pinsky-Rinzel measure of synchrony [121]. We transformed the firing times $T(k)$ for every k^{th} event of the neuron into a set of corresponding vector phases $\phi(k)$ using *Eq. 7*, where $T_{AP}(k)$ corresponds to all the AP events within the duration of simulation. For each vector phase $\phi(k)$, we compute the synchrony $r(\phi(k))$—numbers between 0 and 1—using the complex order parameter defined by Strogatz and Mirollo averaged across all events for a single synaptic configuration [123] (*Eq. 8*).

$$\phi(k) = \frac{T_{AP}(k) - T(k)}{T(k+1) - T(k)} \tag{7}$$

$$r\big(\phi(k)\big) = \frac{1}{N_K} \sum e^{(2\pi i \phi(k))} \tag{8}$$

Numerical Methods

Deterministic equations (*Eqs. 1-4*) are solved using the fourth-order Runge-Kutta algorithm (RK4) with a 1 μs time step, while the stochastic states of the IP_3Rs and VGCCs are determined by the corresponding kinetic schemes were simulated using a procedure outline in [117], which is equivalent to Gillespie algorithm with fixed time step. All numerical simulations were performed in MATLAB (The MathWorks, Natick, MA) and data analysis was carried out using custom Python scripts (version 3.9).

Code availability

The complete model code as well as analysis scripts will be posted on our lab's webpage after the manuscript is accepted for publication.

823

Tables

Table 1. Ca^{2+} fluxes in the model.

Flux (reference)	**Equation**
Basal leak and R/SOCC [110, 111]	$J_{in} = J_{leakin} + V_{leakin} IP_3$
Ca^{2+} diffusion from the IP_3R cluster [67]	$J_{IPR-diff} = k_{IPR-diff}(Ca^{2+}_{IPR_n} - Ca^{2+}_{cyt})$
PMCA [67]	$J_{PMCA} = V_{PMCA} \frac{(Ca^{2+}_{cyt})^n}{(Ca^{2+}_{cyt})^n + {K_{PMCA}}^n}$
SERCA [67]	$J_{SERCA} = V_{SERCA} \frac{(Ca^{2+}_{cyt})^n}{(Ca^{2+}_{cyt})^n + {K_{SERCA}}^n}$
ER-leak [67]	$J_{ER-leak} = k_{ER-leak}(Ca^{2+}_{ER} - Ca^{2+}_{cyt})$
IP_3 Receptor [67]	$J_{IPR} = k_{IPR} P_o (Ca^{2+}_{ER} - Ca^{2+}_{IPR_n})$ $P_o = N_{open}/N_{IP_3R}$
Ca^{2+} diffusion from the VGCC cluster	$J_{VGCC-diff} = k_{VGCC-diff}(Ca^{2+}_{AZ} - Ca^{2+}_{cyt})$
ER—AZ Coupling	$J_{coupling} = V_c \frac{({Ca^{2+}_{AZ}}^2 - \bar{k}({Ca^{2+}_{IP_3R_n}}^2))}{{Ca^{2+}_{AZ}}^2 - {K_c}^2}$
VGCC [6]	$J_{VGCC} = \frac{-I_{Ca^{2+}}}{zFV_{cell}}$ $I_{Ca^{2+}} = channel\ density \cdot cluster\ area \cdot I_s$ $I_s = gP_o(V - E_{Ca^{2+}}),\ P_o = N_{open}/N_{VGCC}$ $channel\ density = \frac{N_{VGCC}}{(AZ_{area} \cdot N_{AZ})}$

829 **Table 2.** Parameter values for the Ca^{2+} dynamics.

Parameters	Description	Value/Units	Notes
Cellular			
J_{leakin}	Plasma membrane leak influx	0.03115 μM·ms^{-1}	From [67]
V_{leakin}	R/SOCC flux coefficient	0.2 ms^{-1}	From [67]
$k_{IPR-diff}$	$Ca^{2+}_{IP_3R_n}$ diffusional flux coefficient	10 ms^{-1}	From [67]
k_{IPR}	IP_3R flux coefficient	5 ms^{-1}	Modified from [67]
N_{IPR}	Total number of IP3R channels	10	
$k_{ER-leak}$	ER-leak flux coefficient	0.0022 ms^{-1}	Modified from [67]
PMCA			
V_{PMCA}	Maximum capacity of PMCA	3.195 μM·ms^{-1}	Modified from [67]
K_{PMCA}	Half activation PMCA constant	0.5 μM	From [67]
n_P	Hill coefficient of PMCA	2	From [67]
SERCA			
V_{SERCA}	Maximum capacity of SERCA	10 μM·ms^{-1}	From [67]
K_{SERCA}	Half maximal activation SERCA constant	0.26 μM	From [67]
n_S	Hill coefficient of SERCA	1.75	From [67]
VGCC and Coupling			
$k_{VGCC-diff}$	Ca^{2+}_{AZ} diffusional flux coefficient	0.071 ms^{-1}	
V_{cell}	Terminal volume	1.22×10^{-6} L	Modified from [6]
$cluster\ area$	Area of VGCC cluster	0.001963 μm^2	Modified from [6]
AZ_{area}	Active zone area	0.04 μm^2	Modified from [2, 6]
N_{AZ}	Active zone number	1.3	Modified from [6]
V_c	Maximum capacity of transfer component	118 μM·ms^{-1}	
$\bar{k}$	Concentrating power of the transfer components.	High coupling: 15 μM	
		Low coupling: 5 μM	
K_c	Half-maximal transfer rate	High coupling: 10 μM	
		Low coupling: 20 μM	

830

831

832 **Table 3.** Additional parameters used in the Ca^{2+} dynamics.

Parameter	**Value / Units**	**Notes**
Resting cytosol [Ca^{2+}]	0.1 μM	
Resting AZ [Ca^{2+}]	0.05 μM	
Resting Total [Ca^{2+}]	56 μM	
Resting [IP_3]	0.1 μM	
Extracellular [Ca^{2+}]	2.0 mM	
δ_1	100	Cytoplasmic to ER microdomain volume ratio
δ_2	10	Cytoplasmic to ER volume ratio
δ_3	60	Cytoplasmic to VGCC microdomain volume ratio

833
834

835 **Table 4.** IP_3 fluxes in the model.

Flux (reference)	**Equation**
PLC_δ [112, 114]	$J_{PLC} = \bar{V}_{PLC} \frac{(Ca_{cyt}^{2+})^2}{(Ca_{cyt}^{2+})^2 + {K_{PLC}}^2}$ $\bar{V}_{PLC} = V_{PLC} PLC$ $V_{PLC} = V_0 + V_Q \frac{q^2}{q^2 + {K_Q}^2}$ $q = H(t - t_1) * A\beta * e^{-r(t-t_1)H(t-t_1)}$ $\rho = V_R \frac{q}{q + K_R}$ $\frac{d}{dt} PLC = k_{f_{PLC}} G(PLC_{tot} - PLC) - k_{b_{PLC}} PLC$ $\frac{d}{dt} G = k_{f_G}(\rho + \delta)(G_{tot} - G) - k_{b_G} G$
IP_3 Degradation [112]	$J_{deg} = \left(\eta \frac{(Ca_{cyt}^{2+})^2}{(Ca_{cyt}^{2+})^2 + {K_{IP_3k}}^2} + (1 - \eta) \right) IP_3$ $\eta = k_{3k}/(k_{3k} + k_{5p})$
Time constant of IP_3 turnover	$\tau_{IP_3} = 1/(k_{3k} + k_{5p})$

836

837 **Table 5.** Transition rates used in the IP_3R model

Rate/parameter	**Equation**
Transition rates	$k_{RA} = \left[1\times\left(\frac{1}{j_{01}[Ca^{2+}]_c} + \frac{1}{j_{12}([Ca^{2+}]_c)^2}\right)\right]^{-1}$ $k_{AR} = \left[K_A([Ca^{2+}]_c)^2\times\left(\frac{1}{j_{01}[Ca^{2+}]_c} + \frac{1}{j_{12}([Ca^{2+}]_c)^2}\right)\right]^{-1}$ $k_{AO} = \left[K_A([Ca^{2+}]_c)^2\times\left(\frac{1}{j_{22}([Ca^{2+}]_c)^2}\right)\right]^{-1}$ $k_{OA} = \left[K_O([Ca^{2+}]_c)^2\times\left(\frac{1}{j_{22}([Ca^{2+}]_c)^2}\right)\right]^{-1}$ $k_{OI} = \left[K_O([Ca^{2+}]_c)^2\times\left(\frac{1}{j_{23}([Ca^{2+}]_c)^3} + \frac{1}{j_{45}([Ca^{2+}]_c)^5}\right)\right]^{-1}$ $k_{IO} = \left[K_I([Ca^{2+}]_c)^5\times\left(\frac{1}{j_{23}([Ca^{2+}]_c)^3} + \frac{1}{j_{45}([Ca^{2+}]_c)^5}\right)\right]^{-1}$ $k_{RI} = \left[1\times\left(\frac{1}{\tilde{j}_{01}[Ca^{2+}]_c} + \frac{1}{\tilde{j}_{45}([Ca^{2+}]_c)^5}\right)\right]^{-1}$ $k_{IR} = \left[K_I([Ca^{2+}]_c)^5\times\left(\frac{1}{\tilde{j}_{01}[Ca^{2+}]_c} + \frac{1}{\tilde{j}_{45}([Ca^{2+}]_c)^5}\right)\right]^{-1}$
Occupancy parameters	$K_O = a_1\frac{[IP_3]^{n_O}}{[IP_3]^{n_O}+K_{Od}{}^{n_O}}$, $K_A = a_2\frac{[IP_3]^{n_A}}{[IP_3]^{n_A}+K_{Ad}{}^{n_A}}$ $K_I = a_2\frac{[IP_3]^{n_I}}{[IP_3]^{n_I}+K_{Id}{}^{n_I}}$

838

839 **Table 6.** Parameter values for the IP_3 dynamics and IP_3R

Parameter	Description	WT	AD	Notes
IP_3 Model				
V_0	PLC-mediated IP_3 production	0.15 μM	0.19 μM	From [114]
V_Q	Control parameter for influence of Aβ on IP_3	7.82 μM	380 μM	From [114]
K_Q	PLC dissociation constant	0.0086 μg/mL	0.0086 μg/mL	From [114]
K_{IP_3k}	Half-activation for 3-kinase	0.6 μM	1.6 μM	From [114]
K_{PLC}	PLC sensitivity to Ca^{2+}	0.01 μM	0.016 μM	From [114]
k_{3k}	IP_3 phosphorylation rate	1.5 μs^{-1}	0.7 μs^{-1}	From [114]
k_{5p}	IP_3 dephosphorylation rate	0.01 μs^{-1}	0.005 μs^{-1}	From [114]
PLC				
$k_{f_{PLC}}$	PLC-protein activation rate	0.35 μs^{-1}	0.75 μs^{-1}	From [114]
$k_{b_{PLC}}$	PLC-protein deactivation rate	22 μs^{-1}	200 μs^{-1}	Modified from [114]
PLC_{tot}	Scaled total number of PLC	1	1	From [114]
G-Protein				
k_{f_G}	G-protein activation rate	0.33 μs^{-1}	0.047 μs^{-1}	From [114]
k_{b_G}	G-protein deactivation rate	2.17 μs^{-1}	4.7 μs^{-1}	From [114]
δ	G-protein intrinsic activity	0.01	0.012	From [114]
V_R	Maximal G-protein activation	7.4	10	From [114]
K_R	Aβ producing half-activation	4467 μg/mL	2000 μg/mL	From [114]
G_{tot}	Scaled total number of G-protein	1	1	From [114]
IP_3R				
a_1		17.05043 μM^{-2}	1.108278×10^{2} μM^{-2}	Fit
n_O		2.473407	2.473407	Fit
K_{Od}		0.909078 μM	0.909078 μM	Fit
a_2		18.49186 μM^{-2}	18.49186 μM^{-2}	Fit
n_A		0.093452	0.093452	Fit
K_{Ad}		1.955650 μM	1.955650 μM	Fit
a_3		2.340259×10^{2} μM^{-5}	1.4041556×10^{2} μM^{-5}	Fit
n_I		56.84823	56.84823	Fit
K_{Id}		0.089938 μM	0.089938 μM	Fit
j_{01}		3.031635×10^{2} $\mu M^{-1}ms^{-1}$	3.031635×10^{2} $\mu M^{-1}ms^{-1}$	Fit
j_{12}		3.230063×10^{2} $\mu M^{-2}ms^{-1}$	3.230063×10^{2} $\mu M^{-2}ms^{-1}$	Fit
j_{22}		4.814111 $\mu M^{-2}ms^{-1}$	5.3978052 $\mu M^{-2}ms^{-1}$	Fit
j_{23}		5.356155 $\mu M^{-3}ms^{-1}$	2.0652269×10^{3} $\mu M^{-3}ms^{-1}$	Fit
j_{45}		5.625616 $\mu M^{-5}ms^{-1}$	5.4319289 $\mu M^{-5}ms^{-1}$	Fit
$\tilde{j}_{01}$		3.013284×10^{2} $\mu M^{-1}ms^{-1}$	3.013284×10^{2} $\mu M^{-1}ms^{-1}$	Fit
$\tilde{j}_{45}$		2.648741 $\mu M^{-5}ms^{-1}$	8.512829×10^{-8} $\mu M^{-5}ms^{-1}$	Fit

840 **Table 7.** Parameter values for membrane potential equations.

Parameter	Value / Units	Description
C_m	1 μF/cm^2	Membrane Capacitance
g_{Na}	120 mS/cm^2	Maximum Conductance for active Na^+ channels
$g_{Na_{leak}}$	0.0175 mS/cm^2	Conductance for Na^+ passive leak channels
g_K	36 mS/cm^2	Maximum Conductance for active K^+ channels
$g_{K_{leak}}$	0.05 mS/cm^2	Conductance for K^+ passive leak channels
$g_{Cl_{leak}}$	0.05 mS/cm^2	Conductance for Cl^- passive leak channels
ϕ	5.0	
g_{AHP}	0.01	
α_n	$\frac{0.01(V+34)}{1-\exp(-\frac{V+34}{10})}$	Forward rate for K^+ current activation gating variable
β_n	$0.125\exp(-\frac{V+44}{80})$	Backward rate for K^+ current activation gating variable
α_h	$0.07\exp(-\frac{V+44}{20})$	Forward rate for Na^+ current inactivation gating variable
β_h	$\frac{1}{1+\exp(-\frac{V+14}{10})}$	Backward rate for Na^+ current inactivation gating variable
α_m	$\frac{0.1(V+30)}{1-\exp(-\frac{V+30}{10})}$	Forward rate for Na^+ current activation gating variable
β_m	$4\exp(-\frac{V+55}{18})$	Backward rate for Na^+ current activation gating variable
m_∞	$\frac{\alpha_m}{\alpha_m+\beta_m}$	Occupancy of Na^+ activation gating variable
	$\frac{dn}{dt}=\phi(\alpha_n(1-n)-\beta_n n)$	Evolution occupancy of gating K^+ current gating variable
	$\frac{dh}{dt}=\phi(\alpha_h(1-h)-\beta_h h)$	Evolution occupancy of gating Na^+ current inactivation gating variable

841

842 **Table 8.** Reaction rates for kinetic schemes for VGCC

Parameter	**Value / Units**	**Notes**
$\alpha_{10}, \alpha_{20}, \alpha_{30}, \alpha_{40}$	4.04, 6.70, 4.39, 17.33 ms^{-1}	From [70, 75]
$\beta_{10}, \beta_{20}, \beta_{30}, \beta_{40}$	2.88, 6.30, 8.16, 1.84 ms^{-1}	From [70, 75]
k_1, k_2, k_3, k_4	49.14, 42.08, 55.31, 26.55 mV	From [70, 75]

843

844

845 **Table 9.** Reaction rates for kinetic schemes for Exocytosis

Parameter	Description	Value / Units	Notes
Vesicle Recruitment			
k_{mob}	Mobilization rate	5.0×10^{-5} $\mu M^{-1} ms^{-1}$	From [27]
k_{demob}	Demobilization rate	0.0022 ms^{-1}	From [27]
$k_{priming}$	Priming rate	0.027990 $\mu M^{-1} ms^{-1}$	From [27]
k_{unpr}	Unpriming rate	0.005356 ms^{-1}	From [27]
k_{attach}	Attachment rate	0.0015 $\mu M^{-1} ms^{-1}$	Fit
k_{detach}	Dettachment rate	0.001158 ms^{-1}	Fit
k_{RF}	Refractoriness	10.34^{-1} ms^{-1}	Fit
Calcium sensor			
α	Association rate for synchronous release	0.061200 $\mu M^{-1} ms^{-1}$	From [70]
β	Dissociation rate, synchronous release	2.32 ms^{-1}	From [70]
λ	Association rate for Asynchronous release	0.002933 $\mu M^{-1} ms^{-1}$	Fit
δ	Dissociation rate for Asynchronous release	0.014829 ms^{-1}	Fit
γ_1	Spontaneous release rate	9×10^{-6} ms^{-1}	Fit
γ_2	Synchronous release rate	2.000008 ms^{-1}	From [70]
γ_3	Asynchronous release rate	$a \cdot \gamma_2$ ms^{-1}	From [70]
b	Cooperativity factor	0.250007	From [70]
a		0.025007	From [70]

846

847 ## Acknowledgements

848 This research was funded by National Institute of Health, grant number R01 AG053988 (to
849 GU and AD)

850

851 ## Competing Interests

852 The authors declare no conflict of interest. The funders had no role in the design of the study;
853 in the collection, analyses, or interpretation of data; in the writing of the manuscript, or in the
854 decision to publish the results.

855

856

857

858

References

1. Sun, J., Pang, Z. P., Qin, D., Fahim, A. T., Adachi, R., & Südhof, T. C. (2007). A dual Ca2+ sensor model for neurotransmitter release in a central synapse. Nature 450, 676—682. https://doi.org/10.1038/nature06308
2. Schikorski, T., & Stevens, C. F. (1997). Quantitative Ultrastructural Analysis of Hippocampal Excitatory Synapses. The Journal of Neuroscience, 17(15), 5858–5867. https://doi.org/10.1523/jneurosci.17-15-05858.1997
3. Sätzler, K., Söhl, L. F., Bollmann, J. H., Borst, J. G. G., Frotscher, M., Sakmann, B., & Lübke, J. H. R. (2002). Three-Dimensional Reconstruction of a Calyx of Held and Its Postsynaptic Principal Neuron in the Medial Nucleus of the Trapezoid Body. The Journal of Neuroscience, 22(24), 10567–10579. https://doi.org/10.1523/jneurosci.22-24-10567.2002
4. Otsu, Y., & Murphy, T. H. (2003). Miniature Transmitter Release: Accident of Nature or Careful Design? Science Signaling, 2003 (211), pe54–pe54. https://doi.org/10.1126/stke.2112003pe54
5. Murthy, V. N., & Stevens, C. F.. (1999). Reversal of synaptic vesicle docking at central synapses. Nature Neuroscience, 2(6), 503–507. https://doi.org/10.1038/9149
6. Ermolyuk, Y. S., Alder, F. G., Surges, R., Pavlov, I. Y., Timofeeva, Y., Kullmann, D. M., & Volynski, K. E.. (2013). Differential triggering of spontaneous glutamate release by P/Q-, N- and R-type Ca2+ channels. Nature Neuroscience, 16(12), 1754–1763. https://doi.org/10.1038/nn.3563
7. De Juan-Sanz, J., Holt, G. T., Schreiter, E. R., De Juan, F., Kim, D. S., & Ryan, T. A.. (2017). Axonal Endoplasmic Reticulum Ca2+ Content Controls Release Probability in CNS Nerve Terminals. Neuron, 93(4), 867–881.e6. https://doi.org/10.1016/j.neuron.2017.01.010
8. Karagas, N. E., & Venkatachalam, K.. (2019). Roles for the Endoplasmic Reticulum in Regulation of Neuronal Calcium Homeostasis. Cells, 8(10), 1232. https://doi.org/10.3390/cells8101232
9. Singh, N., Bartol, T., Levine, H., Sejnowski, T., & Nadkarni, S.. (2021). Presynaptic endoplasmic reticulum regulates short-term plasticity in hippocampal synapses. Communications Biology, 4(1). https://doi.org/10.1038/s42003-021-01761-7

10. Busche, M. A., Chen, X., Henning, H. A., Reichwald, J., Staufenbiel, M., Sakmann, B., & Konnerth, A.. (2012). Critical role of soluble amyloid-β for early hippocampal hyperactivity in a mouse model of Alzheimer's disease. Proceedings of the National Academy of Sciences, 109(22), 8740–8745. https://doi.org/10.1073/pnas.1206171109
11. Stutzmann, G.E, Caccamo. A., LaFerla, F. M., & Parker, I. (2004). Dysregulated IP3 Signaling in Cortical Neurons of Knock-In Mice Expressing an Alzheimer's-Linked Mutation in Presenilin1 Results in Exaggerated Ca2+ Signals and Altered Membrane Excitability. The Journal of Neuroscience 24, 508–513 doi:10.1523/jneurosci.4386-03.2004
12. Zatti, G., Burgo, A., Giacomello, M., Barbiero, L., Ghidoni, R., Sinigaglia, G. & Fasolato, C.. (2006). Presenilin mutations linked to familial Alzheimer's disease reduce endoplasmic reticulum and Golgi apparatus calcium levels. Cell calcium, 39(6), 539-550. doi:10.1016/j.ceca.2006.03.002
13. Berridge, M. J.. (2010). Calcium hypothesis of Alzheimer's disease. Pflügers archiv - european journal of physiology, 459(3), 441-449. doi:10.1007/s00424-009-0736-1
14. Karagas, N. E. & Venkatachalam, K.. (2019). Roles for the Endoplasmic Reticulum in Regulation of Neuronal Calcium Homeostasis. Cells, 8(10), 1232. doi:10.3390/cells8101232
15. Lopez, J. R., Lyckman, A., Oddo, S., Laferla, F. M., Querfurth, H. W. & Shtifman, A.. (2008). Increased intraneuronal resting [Ca2+] in adult Alzheimer's disease mice. Journal of neurochemistry, 105(1), 262-271. doi:10.1111/j.1471-4159.2007.05135.x
16. Mak, D.-O. D., Cheung, K.-H., Toglia, P., Foskett, J. K. & Ullah, G.. (2015). Analyzing and Quantifying the Gain-of-Function Enhancement of IP3 Receptor Gating by Familial Alzheimer's Disease-Causing Mutants in Presenilins. PLOS computational biology, 11(10), e1004529. doi:10.1371/journal.pcbi.1004529
17. Cheung, K.-H., Shineman, D., Müller, M., Cárdenas, C., Mei, L., Yang, J. & Foskett, J. K.. (2008). Mechanism of Ca2+ Disruption in Alzheimer's Disease by Presenilin Regulation of InsP3 Receptor Channel Gating. Neuron, 58(6), 871-883. doi:10.1016/j.neuron.2008.04.015

18. Stanley, E. F.. (1997). The calcium channel and the organization of the presynaptic transmitter release face. Trends in neurosciences, 20(9), 404-409. doi:10.1016/s0166-2236(97)01091-6
19. Chen, M., Van Hook, M. J. & Thoreson, W. B.. (2015). Ca^{2+} Diffusion through Endoplasmic Reticulum Supports Elevated Intraterminal Ca2+ Levels Needed to Sustain Synaptic Release from Rods in Darkness. The journal of neuroscience, 35(32), 11364-11373. doi:10.1523/jneurosci.0754-15.2015
20. Chen, M., Križaj, D., & Thoreson, W.B. (2014). Intracellular calcium stores drive slow non-ribbon vesicle release from rod photoreceptors. Front. Cell. Neurosci. 8, 20 https://doi.org/10.3389/fncel.2014.00020
21. Emptage, N. J., Reid, C. A. & Fine, A.. (2001). Calcium Stores in Hippocampal Synaptic Boutons Mediate Short-Term Plasticity, Store-Operated Ca2+ Entry, and Spontaneous Transmitter Release. Neuron, 29(1), 197-208. doi:10.1016/s0896-6273(01)00190-8
22. Collin, T., Marty, A. & Llano, I.. (2005). Presynaptic calcium stores and synaptic transmission. Current opinion in neurobiology, 15(3), 275-281. doi:10.1016/j.conb.2005.05.003
23. Dobrunz, L. E., Huang, E. P. et Stevens, C. F.. (1997). Very short-term plasticity in hippocampal synapses. Proceedings of the national academy of sciences, 94(26), 14843-14847. doi:10.1073/pnas.94.26.14843
24. Dobrunz, L. E. & Stevens, C. F.. (1997). Heterogeneity of Release Probability, Facilitation, and Depletion at Central Synapses. Neuron, 18(6), 995-1008. doi:10.1016/s0896-6273(00)80338-4
25. Debanne, D., Guérineau, N. C., Gähwiler, B. H. & Thompson, S. M.. (1996). Paired-pulse facilitation and depression at unitary synapses in rat hippocampus: quantal fluctuation affects subsequent release.. The journal of physiology, 491(1), 163-176. doi:10.1113/jphysiol.1996.sp021204
26. Citri, A. & Malenka, R. C.. (2008). Synaptic Plasticity: Multiple Forms, Functions, and Mechanisms. Neuropsychopharmacology, 33(1), 18-41. doi:10.1038/sj.npp.1301559
27. Pan, B. & Zucker, R. S.. (2009). A General Model of Synaptic Transmission and Short-Term Plasticity. Neuron, 62(4), 539-554. doi:10.1016/j.neuron.2009.03.025

28. Neher, E. et Sakaba, T.. (2008). Multiple Roles of Calcium Ions in the Regulation of Neurotransmitter Release. Neuron, 59(6), 861-872. doi:10.1016/j.neuron.2008.08.019
29. Zucker, R. S. & Regehr, W. G.. (2002). Short-Term Synaptic Plasticity. Annual review of physiology, 64(1), 355-405. doi:10.1146/annurev.physiol.64.092501.114547
30. Debanne, D., Guérineau, N. C., Gähwiler, B. H. & Thompson, S. M.. (1996). Paired-pulse facilitation and depression at unitary synapses in rat hippocampus: quantal fluctuation affects subsequent release.. The journal of physiology, 491(1), 163-176. doi:10.1113/jphysiol.1996.sp021204
31. Guo, D. & Li, C.. (2012). Population rate coding in recurrent neuronal networks with unreliable synapses. Cognitive neurodynamics, 6(1), 75-87. doi:10.1007/s11571-011-9181-x
32. Mark S. Goldman. (2004). Enhancement of Information Transmission Efficiency by Synaptic Failures. Neural Comput 16 (6), 1137–1162 doi: https://doi.org/10.1162/089976604773717568
33. Maass, W. & Natschläger, T.. (2000). A Model for Fast Analog Computation Based on Unreliable Synapses. Neural computation, 12(7), 1679-1704. doi:10.1162/089976600300015303
34. Zott, B., Simon, M. M., Hong, W., Unger, F., Chen-Engerer, H.-J., Frosch, M. P. & Konnerth, A.. (2019). A vicious cycle of β amyloid–dependent neuronal hyperactivation. Science, 365(6453), 559-565. doi:10.1126/science.aay0198
35. Busche, M. A., Chen, X., Henning, H. A., Reichwald, J., Staufenbiel, M., Sakmann, B., & Konnerth, A.. (2012). Critical role of soluble amyloid-β for early hippocampal hyperactivity in a mouse model of Alzheimer's disease. Proceedings of the National Academy of Sciences, 109(22), 8740–8745. https://doi.org/10.1073/pnas.1206171109
36. Busche, M. A. & Konnerth, A.. (2015). Neuronal hyperactivity - A key defect in Alzheimer's disease?. Bioessays, 37(6), 624-632. doi:10.1002/bies.201500004
37. Kaeser, P. S. & Regehr, W. G.. (2014). Molecular Mechanisms for Synchronous, Asynchronous, and Spontaneous Neurotransmitter Release. Annual review of physiology, 76(1), 333-363. doi:10.1146/annurev-physiol-021113-170338

38. Hagler, D.J., & Goda, Y. (2001). Properties of synchronous and asynchronous release during pulse train depression in cultured hippocampal neurons. J. Neurophysiol.85, 2324–2334. https://doi.org/10.1152/jn.2001.85.6.2324

39. Yang, L., Wang, B., Long, C., Wu, G. & Zheng, H.. (2007). Increased asynchronous release and aberrant calcium channel activation in amyloid precursor protein deficient neuromuscular synapses. Neuroscience, 149(4), 768-778. doi:10.1016/j.neuroscience.2007.08.025

40. Atluri, P. P. & Regehr, W. G.. (1998). Delayed Release of Neurotransmitter from Cerebellar Granule Cells. The journal of neuroscience, 18(20), 8214-8227. doi:10.1523/jneurosci.18-20-08214.1998

41. Lu, T., & Trussell, L. O.. (2000). Inhibitory Transmission Mediated by Asynchronous Transmitter Release. Neuron, 26(3), 683–694. https://doi.org/10.1016/s0896-6273(00)81204-0Wu

42. Wu, Y., Whiteus, C., Xu, C. S., Hayworth, K. J., Weinberg, R. J., Hess, H. F., & De Camilli, P.. (2017). Contacts between the endoplasmic reticulum and other membranes in neurons. Proceedings of the National Academy of Sciences, 114(24), E4859–E4867. https://doi.org/10.1073/pnas.1701078114

43. Ringsevjen, H., Umbach Hansen, H. M., Hussain, S., Hvalby, Ø., Jensen, V., Walaas, S. I., & Davanger, S.. (2019). Presynaptic increase in IP3 receptor type 1 concentration in the early phase of hippocampal synaptic plasticity. Brain Research, 1706, 125–134. https://doi.org/10.1016/j.brainres.2018.10.030

44. Mattson, M. P., Laferla, F. M., Chan, S. L., Leissring, M. A., Shepel, P. N., & Geiger, J. D.. (2000). Calcium signaling in the ER: its role in neuronal plasticity and neurodegenerative disorders. Trends in Neurosciences, 23(5), 222–229. https://doi.org/10.1016/s0166-2236(00)01548-4

45. Groffen, A. J., Martens, S., Arazola, R. D., Cornelisse, L. N., Lozovaya, N., De Jong, A. P. H., Goriounova, N. A., Habets, R. L. P., Takai, Y., Borst, J. G., Brose, N., Mcmahon, H. T., & Verhage, M.. (2010). Doc2b Is a High-Affinity Ca2+ Sensor for Spontaneous Neurotransmitter Release. Science, 327(5973), 1614–1618. https://doi.org/10.1126/science.1183765

46. Eggermann, E., Bucurenciu, I., Goswami, S. P., & Jonas, P.. (2012). Nanodomain coupling between Ca2+ channels and sensors of exocytosis at fast mammalian synapses. Nature Reviews Neuroscience, 13(1), 7–21. https://doi.org/10.1038/nrn3125

47. Vyleta, N. P., & Smith, S. M.. (2011). Spontaneous Glutamate Release Is Independent of Calcium Influx and Tonically Activated by the Calcium-Sensing Receptor. The Journal of Neuroscience, 31(12), 4593–4606. https://doi.org/10.1523/jneurosci.6398-10.2011

48. Fujii, S., Matsumoto, M., Igarashi, K., Kato, H., & Mikoshiba, K.. (2000). Synaptic Plasticity in Hippocampal CA1 Neurons of Mice Lacking Type 1 Inositol-1,4,5-Trisphosphate Receptors. Learning & Memory, 7(5), 312–320. https://doi.org/10.1101/lm.34100Ringsevjen,

49. H., Umbach Hansen, H. M., Hussain, S., Hvalby, Ø., Jensen, V., Walaas, S. I., & Davanger, S.. (2019). Presynaptic increase in IP3 receptor type 1 concentration in the early phase of hippocampal synaptic plasticity. Brain Research, 1706, 125–134. https://doi.org/10.1016/j.brainres.2018.10.030

50. Nishiyama, M., Hong, K., Mikoshiba, K., Poo, M.-M., & Kato, K.. (2000). Calcium stores regulate the polarity and input specificity of synaptic modification. Nature, 408(6812), 584–588. https://doi.org/10.1038/35046067

51. Ito, E., Oka, K., Etcheberrigaray, R., Nel-son, T. J., McPhie, D. L., Tofel-Grehl,B., et al. (1994). Internal Ca2+mobi-lization is altered in fibroblasts from patients with Alzheimer disease.Proc.Natl. Acad. Sci. U.S.A.91, 534–538.doi: 10.1073/pnas.91.2.534

52. Popugaeva, E., & Bezprozvanny, I.. (2013). Role of endoplasmic reticulum Ca2+ signaling in the pathogenesis of Alzheimer disease. Frontiers in Molecular Neuroscience, 6. https://doi.org/10.3389/fnmol.2013.00029

53. Popugaeva, E., Pchitskaya, E., & Bezprozvanny, I.. (2018). Dysregulation of Intracellular Calcium Signaling in Alzheimer's Disease. Antioxidants & Redox Signaling, 29(12), 1176–1188. https://doi.org/10.1089/ars.2018.7506

54. Hisatsune, C., & Mikoshiba, K.. (2017). IP3receptor mutations and brain diseases in human and rodents. Journal of Neurochemistry, 141(6), 790–807. https://doi.org/10.1111/jnc.13991

55. Kuchibhotla, K. V., Goldman, S. T., Lattarulo, C. R., Wu, H.-Y., Hyman, B. T., & Bacskai, B. J.. (2008). Aβ Plaques Lead to Aberrant Regulation of Calcium Homeostasis In Vivo Resulting in Structural and Functional Disruption of Neuronal Networks. Neuron, 59(2), 214–225. https://doi.org/10.1016/j.neuron.2008.06.008

56. Poejo, J., Salazar, J., Mata, A. M., & Gutierrez-Merino, C.. (2021). The Relevance of Amyloid β-Calmodulin Complexation in Neurons and Brain Degeneration in Alzheimer's Disease. International Journal of Molecular Sciences, 22(9), 4976. https://doi.org/10.3390/ijms22094976

57. Marchenko, S. M., Yarotskyy, V. V., Kovalenko, T. N., Kostyuk, P. G., & Thomas, R. C.. (2005). Spontaneously active and InsP3-activated ion channels in cell nuclei from rat cerebellar Purkinje and granule neurones. The Journal of Physiology, 565(3), 897–910. https://doi.org/10.1113/jphysiol.2004.081299

58. Greotti, E., Capitanio, P., Wong, A., Pozzan, T., Pizzo, P., & Pendin, D.. (2019). Familial Alzheimer's disease-linked presenilin mutants and intracellular Ca2+ handling: A single-organelle, FRET-based analysis. Cell Calcium, 79, 44–56. https://doi.org/10.1016/j.ceca.2019.02.005

59. Hanse, E., & Gustafsson, B.. (2001). Paired-Pulse Plasticity at the Single Release Site Level: An Experimental and Computational Study. The Journal of Neuroscience, 21(21), 8362–8369. https://doi.org/10.1523/jneurosci.21-21-08362.2001

60. Bacaj, T., Wu, D., Yang, X., Morishita, W., Zhou, P., Xu, W., Robert, & Thomas. (2013). Synaptotagmin-1 and Synaptotagmin-7 Trigger Synchronous and Asynchronous Phases of Neurotransmitter Release. Neuron, 80(4), 947–959. https://doi.org/10.1016/j.neuron.2013.10.026

61. Wen, H., Linhoff, M. W., Mcginley, M. J., Li, G.-L., Corson, G. M., Mandel, G., & Brehm, P.. (2010). Distinct roles for two synaptotagmin isoforms in synchronous and asynchronous transmitter release at zebrafish neuromuscular junction. Proceedings of the National Academy of Sciences, 107(31), 13906–13911. https://doi.org/10.1073/pnas.1008598107

62. Geppert M, Goda Y, Hammer RE, Li C, & Rosahl TW, et al. Synaptotagmin I: a major Ca2+ sensor for transmitter release at a central synapse. Cell. 1994; 79:717–727. [PubMed: 7954835]

63. Yang, H., & Xu-Friedman, M. A.. (2010). Developmental Mechanisms for Suppressing the Effects of Delayed Release at the Endbulb of Held. The Journal of Neuroscience, 30(34), 11466–11475. https://doi.org/10.1523/jneurosci.2300-10.2010

64. Otsu, Y.. (2004). Competition between Phasic and Asynchronous Release for Recovered Synaptic Vesicles at Developing Hippocampal Autaptic Synapses. The

Journal of Neuroscience, 24(2), 420–433. https://doi.org/10.1523/jneurosci.4452-03.2004

65. Maximov, A., & Südhof, T. C.. (2005). Autonomous Function of Synaptotagmin 1 in Triggering Synchronous Release Independent of Asynchronous Release. Neuron, 48(4), 547–554. https://doi.org/10.1016/j.neuron.2005.09.006
66. Wang, L.-Y., & Augustine, G. J.. (2015). Presynaptic nanodomains: a tale of two synapses. Frontiers in Cellular Neuroscience, 8. https://doi.org/10.3389/fncel.2014.00455
67. Cao, P., Tan, X., Donovan, G., Sanderson, M. J., & Sneyd, J.. (2014). A Deterministic Model Predicts the Properties of Stochastic Calcium Oscillations in Airway Smooth Muscle Cells. PLOS Computational Biology, 10(8), e1003783. https://doi.org/10.1371/journal.pcbi.1003783
68. Laude, A. J., & Simpson, A. W. M.. (2009). Compartmentalized signalling: Ca2+ compartments, microdomains and the many facets of Ca2+ signalling. The FEBS Journal, 276(7), 1800–1816. https://doi.org/10.1111/j.1742-4658.2009.06927.x
69. Heine, M., Heck, J., Ciuraszkiewicz, A., & Bikbaev, A.. (2020). Dynamic compartmentalization of calcium channel signalling in neurons. Neuropharmacology, 169, 107556. https://doi.org/10.1016/j.neuropharm.2019.02.038
70. Nadkarni, S., Bartol, T. M., Sejnowski, T. J., & Levine, H.. (2010). Modelling Vesicular Release at Hippocampal Synapses. PLOS Computational Biology, 6(11), e1000983. https://doi.org/10.1371/journal.pcbi.1000983
71. Verkhratsky, A.. (2002). The endoplasmic reticulum and neuronal calcium signalling. Cell Calcium, 32(5-6), 393–404. https://doi.org/10.1016/s0143416002001896
72. Deng, P.-Y., Rotman, Z., Jay, Cho, Y., Cui, J., Cavalli, V., Stanislav, & Vitaly. (2013). FMRP Regulates Neurotransmitter Release and Synaptic Information Transmission by Modulating Action Potential Duration via BK Channels. Neuron, 77(4), 696–711. https://doi.org/10.1016/j.neuron.2012.12.018
73. Harraz, F. O., & Altier, C. (2014). STIM1-mediated bidirectional regulation of Ca2+ entry through voltage-gated calcium channels (VGCC) and calcium-release activated channels (CRAC). *Frontiers in molecular neuroscience 8,* **43**
74. Wu, L., & Saggau, P.. (1994). Pharmacological identification of two types of presynaptic voltage- dependent calcium channels at CA3-CA1 synapses of the

hippocampus. The Journal of Neuroscience, 14(9), 5613–5622. https://doi.org/10.1523/jneurosci.14-09-05613.1994

75. Bischofberger, J., Geiger, J. R. P., & Jonas, P.. (2002). Timing and Efficacy of Ca2+Channel Activation in Hippocampal Mossy Fiber Boutons. The Journal of Neuroscience, 22(24), 10593–10602. https://doi.org/10.1523/jneurosci.22-24-10593.2002
76. Mochida, S., Westenbroek, R. E., Yokoyama, C. T., Zhong, H., Myers, S. J., Scheuer, T., Itoh, K., & Catterall, W. A.. (2003). Requirement for the synaptic protein interaction site for reconstitution of synaptic transmission by P/Q-type calcium channels. Proceedings of the National Academy of Sciences, 100(5), 2819–2824. https://doi.org/10.1073/pnas.262787699
77. Kaeser, P. S., Deng, L., Wang, Y., Dulubova, I., Liu, X., Rizo, J., & Südhof, T. C.. (2011). RIM Proteins Tether Ca2+ Channels to Presynaptic Active Zones via a Direct PDZ-Domain Interaction. Cell, 144(2), 282–295. https://doi.org/10.1016/j.cell.2010.12.029
78. Holderith, N., Lorincz, A., Katona, G., Rózsa, B., Kulik, A., Watanabe, M., & Nusser, Z.. (2012). Release probability of hippocampal glutamatergic terminals scales with the size of the active zone. Nature Neuroscience, 15(7), 988–997. https://doi.org/10.1038/nn.3137
79. Keizer, J., & Levine, L.. (1996). Ryanodine receptor adaptation and Ca2+(-)induced Ca2+ release-dependent Ca2+ oscillations. Biophysical Journal, 71(6), 3477–3487. https://doi.org/10.1016/s0006-3495(96)79543-7
80. Zhang, C., Wu, B., Beglopoulos, V., Wines-Samuelson, M., Zhang, D., Dragatsis, I., Südhof, T. C., & Shen, J.. (2009). Presenilins are essential for regulating neurotransmitter release. Nature, 460(7255), 632–636. https://doi.org/10.1038/nature08177
81. Wu, B., Yamaguchi, H., Lai, F. A., & Shen, J.. (2013). Presenilins regulate calcium homeostasis and presynaptic function via ryanodine receptors in hippocampal neurons. Proceedings of the National Academy of Sciences, 110(37), 15091–15096. https://doi.org/10.1073/pnas.1304171110
82. Chakroborty, S., Kim, J., Schneider, C., Jacobson, C., Molgo, J., & Stutzmann, G. E.. (2012). Early Presynaptic and Postsynaptic Calcium Signaling Abnormalities Mask Underlying Synaptic Depression in Presymptomatic Alzheimer's Disease

Mice. The Journal of Neuroscience, 32(24), 8341–8353. https://doi.org/10.1523/jneurosci.0936-12.2012

83. Johenning, F. W., Theis, A.-K., Pannasch, U., Rückl, M., Rüdiger, S., & Schmitz, D.. (2015). Ryanodine Receptor Activation Induces Long-Term Plasticity of Spine Calcium Dynamics. PLOS Biology, 13(6), e1002181. https://doi.org/10.1371/journal.pbio.1002181

84. Arias-Cavieres A. et al. (2018) Ryanodine Receptor-Mediated Calcium Release Has a Key Role in Hippocampal LTD Induction. *Frontiers in cellular neuroscience, 12*. 403 **https://doi.org/10.3389/fncel.2018.00403**

85. Ferri, C. P., Prince, M., Brayne, C., Brodaty, H., Fratiglioni, L., Ganguli, M., Hall, K., Hasegawa, K., Hendrie, H., Huang, Y., Jorm, A., Mathers, C., Menezes, P. R., Rimmer, E., & Scazufca, M.. (2005). Global prevalence of dementia: a Delphi consensus study. The Lancet, 366(9503), 2112–2117. https://doi.org/10.1016/s0140-6736(05)67889-0

86. Reitz, C., & Mayeux, R.. (2014). Alzheimer disease: Epidemiology, diagnostic criteria, risk factors and biomarkers. Biochemical Pharmacology, 88(4), 640–651. https://doi.org/10.1016/j.bcp.2013.12.024

87. Selkoe, D. J.. (2002). Alzheimer's Disease Is a Synaptic Failure. Science, 298(5594), 789–791. https://doi.org/10.1126/science.1074069

88. Shankar, G. M., & Walsh, D. M.. (2009). Alzheimer's disease: synaptic dysfunction and Aβ. Molecular Neurodegeneration, 4(1), 48. https://doi.org/10.1186/1750-1326-4-48

89. Goedert, M., & Crowther, R. A.. (1989). Amyloid plaques, neurofibrillary tangles and their relevance for the study of Alzheimer's disease. Neurobiology of Aging, 10(5), 405–406. https://doi.org/10.1016/0197-4580(89)90076-6

90. Mondragón-Rodríguez, S., Basurto-Islas, G., Santa-Maria, I., Mena, R., Binder, L. I., Avila, J., Smith, M. A., Perry, G., & García-Sierra, F.. (2008). Cleavage and conformational changes of tau protein follow phosphorylation during Alzheimer's disease. International Journal of Experimental Pathology, 89(2), 81–90. https://doi.org/10.1111/j.1365-2613.2007.00568.x

91. Geula, C., Mesulam, M.-M., Saroff, D. M., & Wu, C.-K.. (1998). Relationship Between Plaques, Tangles, and Loss of Cortical Cholinergic Fibers in Alzheimer Disease. Journal of Neuropathology & Experimental Neurology, 57(1), 63–75. https://doi.org/10.1097/00005072-199801000-00008

92. Vogt, L. J. K., Hyman, B. T., Van Hoesen, G. W., & Damasio, A. R.. (1990). Pathological alterations in the amygdala in Alzheimer's disease. Neuroscience, 37(2), 377–385. https://doi.org/10.1016/0306-4522(90)90408-v

93. Hyman, B.T., Van Horsen, G.W., Damasio, A.R., & Barnes, C.L. (1984). Alzheimer's disease: cell-specific pathology isolates the hippocampal formation. *Science 225*, **1168–1170**

94. Ferreiro, E., Oliveira, C. R., & Pereira, C.. (2004). Involvement of endoplasmic reticulum Ca2+ release through ryanodine and inositol 1,4,5-triphosphate receptors in the neurotoxic effects induced by the amyloid-? peptide. Journal of Neuroscience Research, 76(6), 872–880. https://doi.org/10.1002/jnr.20135

95. Kuchibhotla, K. V., Goldman, S. T., Lattarulo, C. R., Wu, H.-Y., Hyman, B. T., & Bacskai, B. J.. (2008). Aβ Plaques Lead to Aberrant Regulation of Calcium Homeostasis In Vivo Resulting in Structural and Functional Disruption of Neuronal Networks. Neuron, 59(2), 214–225. https://doi.org/10.1016/j.neuron.2008.06.008

96. Liang, J., Kulasiri, D., & Samarasinghe, S.. (2015). Ca2+ dysregulation in the endoplasmic reticulum related to Alzheimer's disease: A review on experimental progress and computational modeling. Biosystems, 134, 1–15. https://doi.org/10.1016/j.biosystems.2015.05.003

97. Plácido, A. I., Pereira, C. M. F., Duarte, A. I., Candeias, E., Correia, S. C., Santos, R. X., Carvalho, C., Cardoso, S., Oliveira, C. R., & Moreira, P. I.. (2014). The role of endoplasmic reticulum in amyloid precursor protein processing and trafficking: Implications for Alzheimer's disease. Biochimica Et Biophysica Acta (BBA) - Molecular Basis of Disease, 1842(9), 1444–1453. https://doi.org/10.1016/j.bbadis.2014.05.003

98. Renner, M., Lacor, P. N., Velasco, P. T., Xu, J., Contractor, A., Klein, W. L., & Triller, A.. (2010). Deleterious Effects of Amyloid β Oligomers Acting as an Extracellular Scaffold for mGluR5. Neuron, 66(5), 739–754. https://doi.org/10.1016/j.neuron.2010.04.029

99. Demuro, A., & Parker, I.. (2013). Cytotoxicity of Intracellular A 42 Amyloid Oligomers Involves Ca2+ Release from the Endoplasmic Reticulum by Stimulated Production of Inositol Trisphosphate. The Journal of Neuroscience, 33(9), 3824–3833. https://doi.org/10.1523/jneurosci.4367-12.2013

100. Del Prete, D., Checler, F., & Chami, M.. (2014). Ryanodine receptors: physiological function and deregulation in Alzheimer disease. Molecular Neurodegeneration, 9(1), 21. https://doi.org/10.1186/1750-1326-9-21

101. Bouchard, R., Pattarini, R., & Geiger, J. D.. (2003). Presence and functional significance of presynaptic ryanodine receptors. Progress in Neurobiology, 69(6), 391–418. https://doi.org/10.1016/s0301-0082(03)00053-4

102. Shepherd, G. M. G., & Harris, K. M.. (1998). Three-Dimensional Structure and Composition of CA3→CA1 Axons in Rat Hippocampal Slices: Implications for Presynaptic Connectivity and Compartmentalization. The Journal of Neuroscience, 18(20), 8300–8310. https://doi.org/10.1523/jneurosci.18-20-08300.1998

103. Sharp, A., Mcpherson, P., Dawson, T., Aoki, C., Campbell, K., & Snyder, S.. (1993). Differential immunohistochemical localization of inositol 1,4,5-trisphosphate- and ryanodine-sensitive Ca2+ release channels in rat brain. The Journal of Neuroscience, 13(7), 3051–3063. https://doi.org/10.1523/jneurosci.13-07-03051.1993

104. Bardo, S., Cavazzini, M. G., & Emptage, N.. (2006). The role of the endoplasmic reticulum Ca2+ store in the plasticity of central neurons. Trends in Pharmacological Sciences, 27(2), 78–84. https://doi.org/10.1016/j.tips.2005.12.008

105. Xu, J., Mashimo, T., & Südhof, T. C.. (2007). Synaptotagmin-1, -2, and -9: Ca2+ Sensors for Fast Release that Specify Distinct Presynaptic Properties in Subsets of Neurons. Neuron, 54(4), 567–581. https://doi.org/10.1016/j.neuron.2007.05.004

106. Dodge, F. A., Jr, & Rahamimoff, R. (1967). On the relationship between calcium concentration and the amplitude of the end-plate potential. *The Journal of physiology, 189(2),* **90–92.**

107. Yamamoto, K., & Kobayashi, M.. (2018). Opposite Roles in Short-Term Plasticity for N-Type and P/Q-Type Voltage-Dependent Calcium Channels in GABAergic Neuronal Connections in the Rat Cerebral Cortex. The Journal of Neuroscience, 38(46), 9814–9828. https://doi.org/10.1523/jneurosci.0337-18.2018

108. Neves, G., Cooke, S. F., & Bliss, T. V. P.. (2008). Synaptic plasticity, memory and the hippocampus: a neural network approach to causality. Nature Reviews Neuroscience, 9(1), 65–75. https://doi.org/10.1038/nrn2303

109. Berridge, M. J., Bootman, M. D., & Roderick, H. L.. (2003). Calcium signalling: dynamics, homeostasis and remodelling. Nature Reviews Molecular Cell Biology, 4(7), 517–529. https://doi.org/10.1038/nrm1155

110. Keener, J., & Sneyd, J., Mathematical Physiology I: Cellular Physiology. 2nd ed. Springer Science + Busi-ness Media, LLC; 2009

111. Dupont G, Falcke M, Kirk V, Sneyd J. Models of Calcium Signalling. Springer International Publishing Switzerland; 2016.

112. Politi, A., Gaspers, L. D., Thomas, A. P., & Höfer, T.. (2006). Models of IP3 and Ca2+ Oscillations: Frequency Encoding and Identification of Underlying Feedbacks. Biophysical Journal, 90(9), 3120–3133. https://doi.org/10.1529/biophysj.105.072249

113. Goda, Y., & Stevens, C. F.. (1994). Two components of transmitter release at a central synapse.. Proceedings of the National Academy of Sciences, 91(26), 12942–12946. https://doi.org/10.1073/pnas.91.26.12942

114. Minicucci, J., Alfond, M., Demuro, A., Gerberry, D., & Latulippe, J.. (2021). Quantifying the dose-dependent impact of intracellular amyloid beta in a mathematical model of calcium regulation in xenopus oocyte. PLOS ONE, 16(1), e0246116. https://doi.org/10.1371/journal.pone.0246116

115. Ohana, O., & Sakmann, B.. (1998). Transmitter release modulation in nerve terminals of rat neocortical pyramidal cells by intracellular calcium buffers. The Journal of Physiology, 513(1), 135–148. https://doi.org/10.1111/j.1469-7793.1998.135by.x

116. Rozov, A., Burnashev, N., Sakmann, B., & Neher, E.. (2001). Transmitter release modulation by intracellular Ca 2+ buffers in facilitating and depressing nerve terminals of pyramidal cells in layer 2/3 of the rat neocortex indicates a target cell-specific difference in presynaptic calcium dy. The Journal of Physiology, 531(3), 807–826. https://doi.org/10.1111/j.1469-7793.2001.0807h.x

117. Ullah, G., & Jung, P.. (2006). Modeling the Statistics of Elementary Calcium Release Events. Biophysical Journal, 90(10), 3485–3495. https://doi.org/10.1529/biophysj.105.073460

118. Pijnenburg, Y. A. L., Vd Made, Y., Van Cappellen Van Walsum, A. M., Knol, D. L., Scheltens, P., & Stam, C. J.. (2004). EEG synchronization likelihood in mild cognitive impairment and Alzheimer's disease during a working memory task.

Clinical Neurophysiology, 115(6), 1332–1339. https://doi.org/10.1016/j.clinph.2003.12.029

119. Grady, C. L.. (2001). Altered brain functional connectivity and impaired short-term memory in Alzheimer's disease. Brain, 124(4), 739–756. https://doi.org/10.1093/brain/124.4.739

120. Snyder, E. M., Nong, Y., Almeida, C. G., Paul, S., Moran, T., Choi, E. Y., Nairn, A. C., Salter, M. W., Lombroso, P. J., Gouras, G. K., & Greengard, P.. (2005). Regulation of NMDA receptor trafficking by amyloid-β. Nature Neuroscience, 8(8), 1051–1058. https://doi.org/10.1038/nn1503

121. Pinsky, P. F., & Rinzel, J.. (1995). Synchrony measures for biological neural networks. Biological Cybernetics, 73(2), 129–137. https://doi.org/10.1007/bf00204051

122. Stern, E. A.. (2004). Cortical Synaptic Integration In Vivo Is Disrupted by Amyloid-Plaques. The Journal of Neuroscience, 24(19), 4535–4540. https://doi.org/10.1523/jneurosci.0462-04.2004

123. Strogatz, S. H., & Mirollo, R. E.. (1991). Stability of incoherence in a population of coupled oscillators. Journal of Statistical Physics, 63(3-4), 613–635. https://doi.org/10.1007/bf01029202

124. Leissring, M. A., Paul, B. A., Parker, I., Cotman, C. W., & Laferla, F. M.. (2008). Alzheimer's Presenilin-1 Mutation Potentiates Inositol 1,4,5-Trisphosphate-Mediated Calcium Signaling in Xenopus. Journal of Neurochemistry, 72(3), 1061–1068. https://doi.org/10.1111/j.1471-4159.1999.721061.x

125. Kopell, N., Börgers, C., Pervouchine, D., Malerba, P., Tort, A. (2010). Gamma and Theta Rhythms in Biophysical Models of Hippocampal Circuits. In*: Hippocampal Microcircuits*: *A computational Modeler's Resource Book,* edited by Cutsuridis V, Graham B, Cobb S, Vida I. New York: Springer, **423–457**

126. Khachaturian, Z. S.. (2017). Calcium Hypothesis of Alzheimer's disease and brain aging: A framework for integrating new evidence into a comprehensive theory of pathogenesis. Alzheimer's & Dementia, 13(2), 178. https://doi.org/10.1016/j.jalz.2016.12.006

127. Demuro, A., Mina, E., Kayed, R., Milton, S. C., Parker, I., & Glabe, C. G.. (2005). Calcium Dysregulation and Membrane Disruption as a Ubiquitous Neurotoxic Mechanism of Soluble Amyloid Oligomers*♦. Journal of Biological Chemistry, 280(17), 17294–17300. https://doi.org/10.1074/jbc.m500997200

128. Cheung, K.-H., Mei, L., Mak, D.-O. D., Hayashi, I., Iwatsubo, T., Kang, D. E., & Foskett, J. K.. (2010). Gain-of-Function Enhancement of IP 3 Receptor Modal Gating by Familial Alzheimer's Disease–Linked Presenilin Mutants in Human Cells and Mouse Neurons. Science Signaling, 3(114), ra22–ra22. https://doi.org/10.1126/scisignal.2000818

129. Stutzmann, G. E.. (2006). Enhanced Ryanodine Receptor Recruitment Contributes to Ca2+ Disruptions in Young, Adult, and Aged Alzheimer's Disease Mice. The Journal of Neuroscience, 26(19), 5180–5189. https://doi.org/10.1523/jneurosci.0739-06.2006

130. Sudhof, T. C.. (2012). Calcium Control of Neurotransmitter Release. Cold Spring Harbor Perspectives in Biology, 4(1), a011353–a011353. https://doi.org/10.1101/cshperspect.a011353

131. Eshra, A., Schmidt, H., Eilers, J., & Hallermann, S.. (2021). Calcium dependence of neurotransmitter release at a high fidelity synapse. Elife, 10. https://doi.org/10.7554/elife.70408

132. Delvendahl, I., Weyhersmüller, A., Ritzau-Jost, A., & Hallermann, S.. (2013). Hippocampal and cerebellar mossy fibre boutons - same name, different function. The Journal of Physiology, 591(13), 3179–3188. https://doi.org/10.1113/jphysiol.2012.248294

133. Riascos, D., De Leon, D., Baker-Nigh, A., Nicholas, A., Yukhananov, R., Bu, J., Wu, C.-K., & Geula, C.. (2011). Age-related loss of calcium buffering and selective neuronal vulnerability in Alzheimer's disease. Acta Neuropathologica, 122(5), 565–576. https://doi.org/10.1007/s00401-011-0865-4

134. Kook, S.-Y., Jeong, H., Kang, M. J., Park, R., Shin, H. J., Han, S.-H., Son, S. M., Song, H., Baik, S. H., Moon, M., Yi, E. C., Hwang, D., & Mook-Jung, I.. (2014). Crucial role of calbindin-D28k in the pathogenesis of Alzheimer's disease mouse model. Cell Death & Differentiation, 21(10), 1575–1587. https://doi.org/10.1038/cdd.2014.67

135. Miguel, J. C., Perez, S. E., Malek-Ahmadi, M., & Mufson, E. J. (2021). Cerebellar Calcium-Binding Protein and Neurotrophin Receptor Defects in Down Syndrome and Alzheimer's Disease. Frontiers in aging neuroscience, 13, 645334. https://doi.org/10.3389/fnagi.2021.645334

136. Pchitskaya, E., Popugaeva, E., & Bezprozvanny, I.. (2018). Calcium signaling and molecular mechanisms underlying neurodegenerative diseases. Cell Calcium, 70, 87–94. https://doi.org/10.1016/j.ceca.2017.06.008

137. De Young, G. W., & Keizer, J.. (1992). A single-pool inositol 1,4,5-trisphosphate-receptor-based model for agonist-stimulated oscillations in Ca2+ concentration.. Proceedings of the National Academy of Sciences, 89(20), 9895–9899. https://doi.org/10.1073/pnas.89.20.9895

138. Shuai, J., Pearson, J. E., Foskett, J. K., Mak, D.-O. D., & Parker, I.. (2007). A Kinetic Model of Single and Clustered IP3 Receptors in the Absence of Ca2+ Feedback. Biophysical Journal, 93(4), 1151–1162. https://doi.org/10.1529/biophysj.107.108795

139. Ullah, G., Daniel Mak, D.-O., & Pearson, J. E.. (2012). A data-driven model of a modal gated ion channel: The inositol 1,4,5-trisphosphate receptor in insect Sf9 cells. Journal of General Physiology, 140(2), 159–173. https://doi.org/10.1085/jgp.201110753

140. Cai, Q., & Tammineni, P.. (2017). Mitochondrial Aspects of Synaptic Dysfunction in Alzheimer's Disease. Journal of Alzheimer's Disease, 57(4), 1087–1103. https://doi.org/10.3233/jad-160726

141. Du, H., Guo, L., Yan, S., Sosunov, A. A., Mckhann, G. M., & Shidu Yan, S. (2010). Early deficits in synaptic mitochondria in an Alzheimer's disease mouse model. Proceedings of the National Academy of Sciences, 107 (43), 18670–18675 https://doi.org/10.1073/pnas.1006586107